Iodine chemistry in the chemistry-climate model SOCOL-AERv2-I

Arseniy Karagodin-Doyennel[1,2,*], Eugene Rozanov[1,2,3,*], Timofei Sukhodolov[1,2,3,*],
Tatiana Egorova[2,*], Alfonso Saiz-Lopez[4], Carlos A. Cuevas[4], Rafael P. Fernandez[4,5],
Tomás Sherwen[6,7], Rainer Volkamer[1,8,9,10], Theodore K. Koenig[8,9], Tanguy Giroud[1], and
Thomas Peter[1]

[1]The Institute for Atmospheric and Climate Science (IAC) ETH, Zurich, Switzerland
[2]The Physikalisch-Meteorologisches Observatorium Davos/World Radiation Center (PMOD/WRC), Davos, Switzerland
[3]Saint Petersburg State University, Saint Petersburg, Russia
[4]Department of Atmospheric Chemistry and Climate, IQFR-CSIC, Spain
[5]Institute for Interdisciplinary Science, National Research Council (ICB-CONICET), FCEN-UNCuyo, Mendoza, Argentina
[6]National Centre for Atmospheric Science, University of York, York, YO10 5DD, UK
[7]Wolfson Atmospheric Chemistry Laboratories, University of York, York, YO10 5DD, UK
[8]Department of Chemistry, University of Colorado Boulder, Boulder, CO 80309
[9]Cooperative Institute for Research in Environmental Sciences, Boulder, CO 80309
[10]Laboratory of Radiochemistry and Environmental Chemistry, Paul Scherrer Institute, 5232 Villigen, Switzerland
[*]These authors contributed equally to this work.

Correspondence: Arseniy Karagodin-Doyennel (darseni@student.ethz.ch)

Abstract. In this paper, we present a new version of the chemistry-climate model SOCOL-AERv2 supplemented by an iodine chemistry module. We perform three twenty-year ensemble experiments to assess the validity of the modeled iodine and to quantify the effects of iodine on ozone. The iodine distributions obtained with SOCOL-AERv2-I agree well with AMAX-DOAS observations and with CAM-chem model simulations. For the present-day atmosphere, the model suggests that the iodine-induced chemistry leads to a 3-4% reduction in the ozone column, which is greatest at high latitudes. The model indicates the strongest influence of iodine in the lower stratosphere with 30 ppbv less ozone at low latitudes and up to 100 ppbv less at high latitudes. In the troposphere, the account of the iodine chemistry reduces the tropospheric ozone concentration by 5-10% depending on geographical location. In the lower troposphere, 75% of the modeled ozone reduction originates from inorganic sources of iodine, 25% from organic sources of iodine. At 50 hPa, the results show that the impacts of iodine from both sources are comparable. Finally, we determine the sensitivity of ozone to iodine by applying a 2-fold increase in iodine emissions, as it might be representative for iodine by the end of this century. This reduces the ozone column globally by an additional 1.5-2.5%. Our results demonstrate the sensitivity of atmospheric ozone to iodine chemistry for present and future conditions, but uncertainties remain high due to the paucity of observational data of iodine species.

1 Introduction

Emissions of chlorine- and bromine-containing halogen compounds have long been the subject of scientific investigation because they play an important role in the catalytic destruction cycles of stratospheric ozone (Solomon, 1999). Recent studies demonstrate the success of the Montreal Protocol and its Amendments in phasing out the emissions of chlorine- and bromine-

containing substances and also point to early signs of stratospheric ozone recovery (e.g., Newman et al., 2009; Egorova et al., 2013; WMO, 2018). At the same time, our understanding of iodine-induced ozone depletion is incomplete because of the extremely low stratospheric iodine concentrations, typically in the parts-per-trillion (pptv) range (Solomon et al., 1994; Saiz-Lopez et al., 2012). However, the ozone depletion efficiency of iodine-containing species on a per-molecule basis is hundreds of times higher than that of chlorine (Solomon et al., 1994; Gutmann et al., 2018; Koenig et al., 2020), because iodine reservoir species readily convert to free radicals, I and IO, in the presence of sunlight. Therefore, iodine chemistry remains suspected of affecting stratospheric ozone (Saiz-Lopez et al., 2015) and slowing the recovery of the ozone layer (Koenig et al., 2020). Still, iodine-induced ozone depletion is not regulated under the Montreal Protocol as the mixing ratio of total inorganic iodine in the atmosphere is extremely low ($\sim$ 1 pptv) and because there is almost no direct anthropogenic production of iodine-containing species (Fuge and Johnson, 2015).

The study of iodine source gases (ISGs) began in the late 1970s. The main organic source of atmospheric iodine is found to be iodomethane (CH_3I) as suggested by Lovelock and Maggs (1973) and Chameides and Davis (1980). Photochemical production in ocean surface water involving phytoplankton and algae is the main source of organic and inorganic iodine that enters the atmosphere (Saiz-Lopez et al. (2012) and references therein). Iodocarbons are further emitted by wetland plants (Manley et al., 2007), biomass burning (Akagi et al., 2011), rice paddies (Lee-Taylor and Redeker, 2005), and volcanoes (Bureau et al., 2000; Aiuppa et al., 2005). ISGs are produced mostly in the tropics as the sea surface temperature (SST) is an important driver of biological activity. The 5-6 day lifetime of CH_3I is long enough to allow a small fraction of it to reach the upper troposphere via tropical convection with an estimated mixing ratio $\sim$ 0.1 pptv in the tropical tropopause layer (WMO, 2018). Other organic ISGs, such as CH_2I_2, CH_2ICl, CH_2IBr, and C_2H_5I, are only minor contributors to iodine abundance in the upper troposphere and stratosphere since their lifetimes after volatilization are just a few hours on average.

Knowledge of the sources of atmospheric iodine has changed when the importance of inorganic iodine emissions was recognized, such as molecular iodine, I_2 (Saiz-Lopez and Plane, 2004), and hypoiodous acid, HOI (Carpenter et al., 2013). These are formed through reactions of near-surface ozone with oceanic iodide (I^-), i.e. $O_3 + H^+ + I^- \longrightarrow HOI + O_2$ and $HOI + H^+ + I^- \longrightarrow I_2 + H_2O$, which are possibly responsible for up to 75% of total iodine emissions (Carpenter et al., 2013; Prados-Roman et al., 2015b). In conjunction with these findings, (MacDonald et al., 2014) used a numerical parametrization of sea-surface iodide in numerical modeling of HOI and I_2 fluxes. Caused by the growing anthropogenic air pollution and the concomitant increase in surface ozone levels, iodine emissions have risen continuously during the past decades. Cuevas et al. (2018) and Legrand et al. (2018) argued that the atmospheric iodine loading must have increased by at least a factor of 3 since the 1950s, because of increasing anthropogenic NO_x emissions resulting in an increase in near-surface ozone. This is in addition to a simultaneous increase in SST due to global warming with correspondingly enhanced metabolic rates of oceanic biota. While the future surface ozone evolution has a large spread in model projections covering the 21st century (Archibald et al., 2020), which results in large uncertainty in future iodine emissions, the continuous increase in surface temperatures is predicted to raise tropospheric iodine levels throughout the 21st century based on Representative Concentration Pathway (RCP) scenarios

(Iglesias-Suarez et al., 2020). In addition, the effectiveness of iodine for ozone depletion (O_3 destruction by one I atom relative to O_3 destruction by one Cl atom) is predicted to change, with the share of halogen-induced ozone loss due to reactions of

55   iodine likely to grow in the future stratosphere (Klobas et al., 2021).

Using a two-dimensional model of atmospheric chemistry and dynamics, Solomon et al. (1994) demonstrated a high impact of iodine chemistry on ozone even when only 1 pptv of total stratospheric iodine is present. These model results were later put in perspective by Pundt et al. (1998), who presented an upper limit of concentration of reactive IO of less than 0.1-

60   0.2 pptv in the upper troposphere-lower stratosphere measured during nine balloon flights over Scandinavia and France. This suggested only a small influence of iodine chemistry on stratospheric ozone. In contrast, using differential optical absorption spectroscopy (DOAS) Wittrock et al. (2000) found significant concentrations of IO between 0.65 and 0.8 pptv (+/- 0.2 pptv) over Spitsbergen Island. Recent aircraft campaigns, also applying DOAS (Baidar et al., 2013) over the West Pacific during CONTRAST (Convective Transport of Active Species in the Tropics) in January–February 2014 (Pan et al., 2017) and over the

65   East Pacific during TORERO (Tropical Ocean Troposphere Exchange of Reactive Halogen Species and Oxygenated VOC) in January–February 2012 (Volkamer et al., 2015)[1] measured a second maximum in IO mixing ratio of more than 0.1 pptv in the tropical tropopause layer that had not been observed before. Yet, globally representative quantitative measurements of iodine species are still not available. Quasi-global IO has been inferred from the SCIAMACHY satellite measurements (Schönhardt et al., 2008), though with a very high level of uncertainty.

70

Modeling of atmospheric iodine chemistry started with Vogt et al. (1996, 1999) proposing a detailed iodine chemistry scheme with gas and aqueous phase reactions in a box model, allowing iodine species to recycle via the uptake of HOI onto sea-salt particles resulting in the production of ICl and IBr (i.e., $HOI + Cl^- + H^+ \rightarrow ICl + H_2O$, $HOI + Br^- + H^+ \rightarrow IBr + H_2O$). Note that these recycling reactions constitute a net source of bromine and chlorine into the atmosphere but represent only a

75   change in partitioning for the iodine species, which avoids iodine uptake and washout (e.g., as $H^+ + I^-$). Dix et al. (2013) hypothesized that the measured increase of IO mixing ratio in the Pacific free troposphere might hint at heterogeneous recycling processes from aerosols back to the gas phase in the upper troposphere. Ordóñez et al. (2012) were the first to use a global chemistry-climate model, namely CAM-chem, to incorporate a comprehensive bromine and iodine chemistry scheme. The global distribution of organic iodocarbons from CAM-chem showed reasonable agreement with observations in the marine

80   boundary layer when including global oceanic ISGs of approximately 1.9 Tg(I)/yr (Prados-Roman et al., 2015a,b). Later, an updated version of the GEOS-Chem model (Sherwen et al., 2016a) demonstrated 3.83 Tg (I)/year of total ISGs emissions, when using the sea-surface iodide field from Chance et al. (2014). Sherwen et al. (2016c) used the sea-surface values from MacDonald et al. (2014), which possibly underestimates the sea-surface iodide emissions in comparison to observations (Sherwen et al., 2019), suggesting only 2.7 Tg (I)/year of total emissions. In order to reproduce the IO observations of Volkamer

85   et al. (2015), Saiz-Lopez et al. (2015) introduced the heterogeneous recycling of iodine reservoirs (HOI and $IONO_2$) on ice crystals, and implemented it in CAM-chem, assuming it to be analogous to bromine recycling on ice crystals in the upper

---

[1] The GV AMAX-DOAS Data can be found here: https://data.eol.ucar.edu/

troposphere (Aschmann and Sinnhuber, 2013). Accordingly, the total iodine injected into the stratosphere is currently thought to be up to 0.8 pptv (WMO, 2018), i.e. about five times larger than that from the previously published assessment (WMO, 2014). Also, CAM-chem results suggest that stratospheric iodine might be responsible for up to 30% of halogen-mediated ozone depletion in the lower tropical stratosphere. At the same time, the results of Hossaini et al. (2015) obtained using the 3-D chemistry transport model TOMCAT suggest that iodine lowers stratospheric ozone only by ∼3% and total column ozone by 0.5%. However, this model did not take the recycling mechanism described in Saiz-Lopez et al. (2015) into consideration, which increases the stratospheric iodine levels significantly beyond what was assumed by Hossaini et al. (2015). It remains difficult to judge which results are closer to reality because of the paucity of observations.

This paper introduces the new version of the chemistry-climate model (CCM) SOCOL-AERv2 (Solar Climate Ozone Links coupled to a size-resolving sulfate aerosol module), which has been extended to include an iodine chemistry scheme. The main objective of this study is to verify the model and further constrain the impact of iodine chemistry on stratospheric ozone depletion, first based on present-day emissions, and second when applying a 2-fold increase of iodine emissions. Section 2 provides a short description of SOCOL-AERv2 (2.1), improvements which have been made to obtain the new model version subsequently referred to as SOCOL-AERv2-I (2.2), and describes the numerical experiments conducted with the new model version (2.3). Section 3 presents the model results, i.e. the comparison of simulated and observed iodine, as well as first, different aspects of iodine effect on present-day stratospheric ozone climatology, are considered (3.1), and second, the sensitivity of ozone to iodine is presented (3.2). Finally, the discussion and summary of the present study are provided in Section 4.

2 Model description and conducted experiments

2.1 The SOCOL-AERv2 chemistry-climate model

The chemistry-climate model SOCOL-AERv2 is the CCM SOCOLv3 (Stenke et al., 2012; Revell et al., 2015) coupled to a size-resolving sulfate aerosol module (AER) (Weisenstein et al., 1997) along with other important modifications for chemistry and deposition. The AER module of SOCOL was established by Sheng et al. (2015) (CCM SOCOL-AERv1). The CCM SOCOL-AERv1 was substantially updated by Feinberg et al. (2019) (CCM SOCOL-AERv2) with an interactive deposition scheme, expanding tropospheric chemistry scheme, and improved sulfate mass and particle number conservation (less susceptible to numerical diffusion). The SOCOL-AERv2 consists of a dynamical core that is the middle atmosphere version of the spectral transform general circulation model MA-ECHAM5.4 (the Middle Atmosphere version of the European Centre/Hamburg Model version 5.4) (Manzini et al., 2006), which has been interactively coupled to the MEZON atmospheric chemistry-transport module (Model for the Evaluation of OZONe Trends) (Egorova et al., 2003). The coupling takes account of radiative forcing caused by ozone, H_2O, N_2O, CH_4, and CFCs. The MA-ECHAM developed at the Max Planck Institute for Meteorology (Hamburg, Germany) is based on primitive prognostic equations for meteorological parameters such as logarithm of surface pressure, temperature, humidity, vorticity, etc. The advection in MA-ECHAM is regulated by a flux-transform semi-Lagrangian scheme based on mass conservation and shape retention (Lin and Rood, 1996). The standard SOCOL-AERv2 utilizes the

120   Gaussian transform horizontal grid with T42 triangular truncation (64 latitudes $\times$ 128 longitudes) splitting the model space into grid cells of $\sim$ 2.5 $\times$ 2.5 degrees each. The vertical direction model grid consists of 39 levels in the hybrid sigma-pressure coordinate system covering the altitudes ranging from the ground surface and 0.01 hPa or about 80 km. The model time step is 15 min for dynamical and physical processes whereas it is 2 hours for atmospheric full radiation and chemical calculations. The CCM SOCOL-AERv2 uses the prescribed monthly fields of the sea surface temperature (SST) and ice coverage acquired

125   from the Hadley Centre dataset (Rayner et al., 2003). MEZON shares the horizontal and vertical spatial resolutions with MA-ECHAM5 and includes 95 chemical species, 215 gas-phase, 16 heterogeneous, and 75 photolysis reactions. For more details on CCM SOCOL-AERv2, see Feinberg et al. (2019).

2.2   SOCOL-AERv2 updates to SOCOL-AERv2-I

Here, we introduce the SOCOL-AERv2-I that is the SOCOL-AERv2 extended with the iodine chemistry module. This module

130   includes 61 gas-phase and 4 heterogeneous chemical reactions involving iodine, boundary conditions for prescribed iodocarbon emissions, interactive inorganic iodine emissions, wet/dry depositions of iodine species augmented with the deposition on sea-salt and sulfate aerosol particles as well as effective uptake (removal)/reactive uptake (recycling) on tropospheric cloud ice. The following section describes all components of the iodine chemistry module in SOCOL-AERv2-I. The prescribed organic and interactive inorganic iodine source gases (ISGs) are presented in Table 1.

Table 1: Iodine source gases (ISGs) incorporated in SOCOL-AERv2-I

ISG	Type	Resolution	Reference
I_2	interactive	model time step	Carpenter et al. (2013)
HOI	interactive	model time step	Carpenter et al. (2013)
CH_3I	prescribed	monthly	Ordóñez et al. (2012)
CH_2I_2	prescribed	monthly	Ordóñez et al. (2012)
CH_2ICl	prescribed	monthly	Ordóñez et al. (2012)
CH_2IBr	prescribed	monthly	Ordóñez et al. (2012)

135   Following Ordóñez et al. (2012), the organic iodocarbons have been obtained from the inventory of Bell et al. (2002) for CH_3I and from the 1-D model estimates of Jones et al. (2010) for CH_2I_2, CH_2ICl, and CH_2IBr. Organic ISGs have been parameterized in Ordóñez et al. (2012) by a biogenic chlorophyll-α (chl-α) dependent source in the tropical oceans (McClain et al., 2004). In our scheme, organic emissions are prescribed on the monthly basis. To simulate the long-term period, we repeat organic emissions fluxes at the beginning of every model year, so any interannual variability is not included.

140   Iodocarbon source fluxes were directly extracted from the GEOS-Chem model (v10-01) at a resolution of a 2 $\times$ 2.5 degrees including updates to both iodine and bromine chemistry from Sherwen et al. (2016c) and Schmidt et al. (2016), and interpolated on the SOCOL-AERv2-I horizontal grid (T42). The inorganic HOI/I_2 fluxes are interactively calculated in the model using

the numerical parametrization of Carpenter et al. (2013) and global sea surface iodide concentration calculated following MacDonald et al. (2014). To derive HOI/I_2 fluxes this parametrization utilizes the model fields of near-surface ozone (at closest to the surface model level), surface wind speed, and SST.

The parametrization for the emission fluxes of F_{HOI} and F_{I_2} (in nmol m^{-2} d^{-1}) as function of the surface ozone mixing ratio $\chi_{O_{3,surf}}$ (in ppbv) are given by

$$F_{HOI} = \chi_{O_{3,surf}} \times (4.15 \times 10^5 \times (M_{I_{aq}^-}^{1/2}/W_s) - (20.6/W_s) - 23600 \times M_{I_{aq}^-}^{1/2}), \tag{1}$$

$$F_{I_2} = \chi_{O_{3,surf}} \times M_{I_{aq}^-}^{1.3} \times (1.74 \times 10^9 - 6.54 \times 10^8 \times \ln W_s), \tag{2}$$

where W_s is the surface wind speed (in m s^{-1}) and $M_{I_{aq}^-}$ is the sea surface iodide concentration expressed as molarity (mol dm^{-3})

$$M_{I_{aq}^-} = 1.46 \times 10^6 \exp(-9134/T_{ss}) \tag{3}$$

with sea surface temperature T_{ss} in K.

It is important to note that this parameterization is intended for calculating I_2 and HOI fluxes at wind speeds below 14 m s^{-1} (higher wind speeds lead to negative values of fluxes) since it is based on the approximation of measurements and there are no measurements when a storm occurs. Also, it should be mentioned that turbulent mixing of the interfacial layer with bulk seawater reduces the proportion of I_2 and HOI evading into the atmosphere therefore fluxes decrease with the wind speed (MacDonald et al., 2014). The obtained inorganic ISGs fluxes in the SOCOL-AERv2-I exceed GEOS-Chem and CAM-Chem emissions because SOCOL-AERv2-I overestimates near-surface O_3 (Revell et al., 2018). When we compared the ground-level ozone fields from SOCOL and GEOS-chem, we found that for most of all regions where HOI/I_2 emissions are produced, the overestimation of ground-level ozone in SOCOL is ~100%. To ameliorate this bias, the surface ozone used within the parameterization was scaled by 0.5. This halved the emission giving HOI/I_2 fluxes comparable: $\sim$ 2.4 Tg (I)/year in SOCOL-AERv2-I and $\sim$ 2.2 Tg (I)/year in GEOS-chem (Sherwen et al., 2016c). Since there is an uncertainty in inorganic iodine emissions (Chance et al., 2014; Sherwen et al., 2016c), such a difference in emissions between models is admissible. Iodocarbon source fluxes in both SOCOL-AERv2-I and GEOS-chem are identical and correspond to 0.5 Tg (I)/year. Iodine emission fluxes used in CCM SOCOL-AERv2-I are demonstrated in Figure 1.
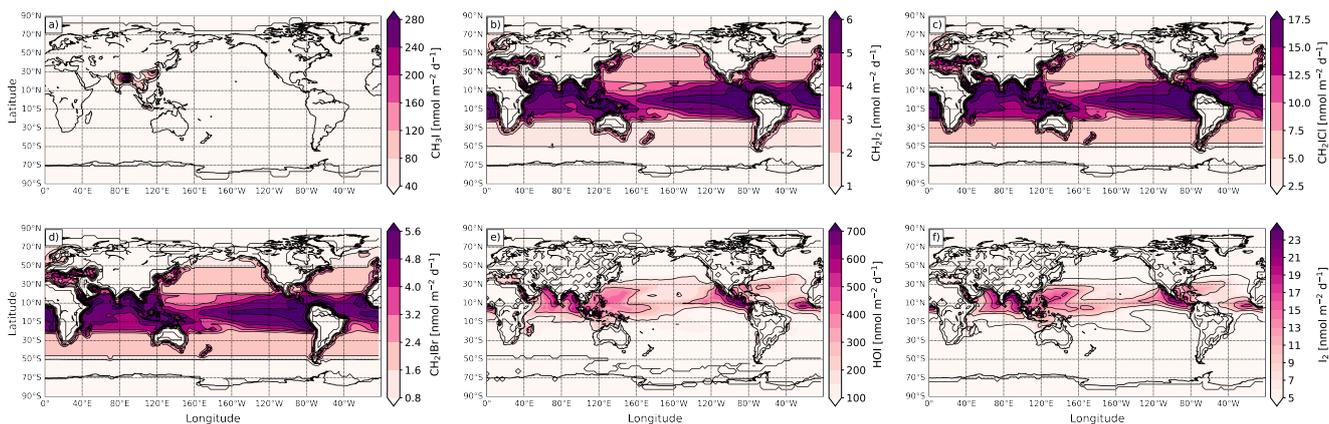
Figure 1. Annual-mean emission fluxes of organic (CH_3I (a), CH_2I_2 (b), CH_2ICl (c), and CH_2IBr (d)) and inorganic (HOI (e) and I_2 (f)) iodine source gases [in nmol m^{-2} d^{-1}] used in SOCOL-AERv2-I.

As it is seen in Figure 1, the sum inorganic fluxes of ISGs [HOI + I_2] is roughly three times higher than that of organic fluxes [$CH_3I + CH_2I_2 + CH_2ICl + CH_2IBr$] of ISGs that is corresponding well with Carpenter et al. (2013).

170   Chemical compounds involved in the iodine chemistry scheme in SOCOL-AERv2-I are presented in Table 2.

Table 2: The iodine species considered in SOCOL-AERv2-I

Species	Molar mass (g mol^{-1})	Henry's law constant (H) (mol m^{-3} atm^{-1})	Temperature dependence of H (K)	Reference
I	126.90	7.9×10^1	0	Burkholder et al. (2015)
I_2	253.81	2.8×10^3	3900	Burkholder et al. (2015)
IO	142.90	—	—	—
OIO	158.90	—	—	—
INO_2	172.91	3.0×10^2	0	Ordóñez et al. (2012)
INO	156.91	—	—	—
$IONO_2$	188.91	∞	0	Burkholder et al. (2015)
HOI	143.91	4.1×10^5	0	Badia et al. (2019)
HI	127.91	7.3×10^{16}	3190	Badia et al. (2019)
IBr	206.81	2.43×10^4	0	Wagman et al. (1989)
ICl	162.36	1.1×10^5	0	Wagman et al. (1989)
I_2O_2	285.81	∞	0	Badia et al. (2019)
I_2O_3	301.81	∞	0	Badia et al. (2019)
I_2O_4	317.81	∞	0	Badia et al. (2019)

7

CH$_3$I	141.94	2.0×10^2	3600		Burkholder et al. (2015)
CH$_2$I$_2$	267.84	7.3×10^3	0		Burkholder et al. (2015)
CH$_2$I	140.93	—	—		—
CH$_2$IBr	220.83	2.0×10^3	0		Hilal et al. (2008)
CH$_2$ICl	176.38	2.0×10^3	0		Hilal et al. (2008)

A dash means that Henry's law constant is unavailable;

For IONO$_2$ and I$_x$O$_y$ Henry's law constants are assumed to be infinity and represented by a very large number.

Overall, 19 iodine species are included in the current version of the iodine chemistry scheme of SOCOL-AERv2-I: 6 iodine source gases (ISGs), 13 product gases (PGs) including two species (HOI and I$_2$), which are both being emitted and chemically produced. Photolysis rates and reaction cross-sections for iodine species were taken from Burkholder et al. (2015). An exception is made only for the photolysis rates of higher iodine oxides species, such as I$_2$O$_2$, I$_2$O$_3$, and I$_2$O$_4$, where we followed the recommendations of Davis et al. (1996) and Vogt et al. (1999), who suggested using photolysis rates of higher iodine oxides nine times higher than those of Cl$_2$O$_2$. This is a more simplified approach than used in CAM-chem, where cross-sections for I$_2$O$_2$ and I$_2$O$_3$ are adopted from Gómez-Martín et al. (2005) and for I$_2$O$_4$, the used spectrum is measured at the University of Leeds (Saiz-Lopez et al., 2014). In GEOS-chem, the cross-sections for higher iodine oxides are equal to those of IONO$_2$ (Sherwen et al., 2016a) based on the assumption made by Bloss et al. (2010). In our scheme, we checked this possibility too and found that there is no noticeable difference between using IONO$_2$ photolysis rates or 9*Cl$_2$O$_2$ photolysis rates as substitutes for unknown photolysis rates of higher iodine oxides. The Henry's law constant of IONO$_2$ is taken in SOCOL-AERv2-I to be infinity by analogous to BrONO$_2$ and ClONO$_2$ (1×10^{30} mol m^{-3} atm^{-1}). The Henry's law constant of I$_x$O$_y$ is infinity and represented by 2.65×10^{18} mol m^{-3} atm^{-1} (Badia et al., 2019). The Henry's law constant of INO$_2$ is equal to that of BrNO$_2$ presented in Ordóñez et al. (2012).

The full iodine reaction scheme, composed of 61 gas-phase chemical reactions including 17 photolysis reactions and 4 heterogeneous reactions proceeding on tropospheric cloud ice is presented in Table 3.

Table 3: The list of chemical reactions with iodine included to SOCOL-AERv2-I

Part 1: Gas-phase chemical reactions.

Chemical reaction	A-factor [cm^{-3} molecule^{-1} s^{-1}]	E$_a$/R (K)	Reference
I$_2$ + O$_3$ → IO + I + O$_2$	3.8×10^{-18}	—	Ordóñez et al. (2012)
I$_2$ + O$_3$ → OIO + IO	3.8×10^{-18}	—	Ordóñez et al. (2012)
I + O$_3$ → IO + O$_2$	2.3×10^{-11}	870	Burkholder et al. (2015)
I + HO$_2$ → HI + O$_2$	1.5×10^{-11}	1090	Ordóñez et al. (2012)

Reaction	Rate		Reference
$IO + NO \rightarrow I + NO_2$	9.1×10^{-12}	-240	Burkholder et al. (2015)
$IO + HO_2 \rightarrow HOI + O_2$	1.3×10^{-11}	-570	Burkholder et al. (2015)
$IO + IO \rightarrow OIO + I$	2.13×10^{-11}	-180	Saiz-Lopez et al. (2014)
$IO + IO \rightarrow I_2O_2$	3.24×10^{-11}	-180	Badia et al. (2019)
$I_2 + OH \rightarrow HOI + I$	1.8×10^{-10}	—	Burkholder et al. (2015)
$I_2 + NO_3 \rightarrow I + IONO_2$	1.5×10^{-12}	—	Saiz-Lopez et al. (2014)
$I + NO_3 \rightarrow IO + NO_2$	1.0×10^{-10}	—	Badia et al. (2019)
$OH + HI \rightarrow I + H_2O$	1.6×10^{-11}	440	Badia et al. (2019)
$HOI + OH \rightarrow IO + H_2O$	2.0×10^{-13}	—	Saiz-Lopez et al. (2014)
$INO + INO \rightarrow I_2 + NO + NO$	8.4×10^{-11}	2620	Burkholder et al. (2015)
$INO_2 + INO_2 \rightarrow I_2 + NO_2 + NO_2$	2.9×10^{-11}	2600	Burkholder et al. (2015)
$IO + BrO \rightarrow Br + I + O_2$	3.0×10^{-12}	-510	Badia et al. (2019)
$IO + BrO \rightarrow Br + OIO$	1.2×10^{-11}	-510	Badia et al. (2019)
$I + BrO \rightarrow IO + Br$	1.44×10^{-11}	—	Saiz-Lopez et al. (2014)
$IO + ClO \rightarrow I + Cl + O_2$	1.175×10^{-12}	-280	Saiz-Lopez et al. (2014)
$IO + O \rightarrow I + O_2$	1.4×10^{-10}	—	Burkholder et al. (2015)
$O + I_2 \rightarrow IO + I$	1.4×10^{-10}	0	Burkholder et al. (2015)
$OH + CH_3I \rightarrow CH_2I + H_2O$	2.9×10^{-12}	1100	Burkholder et al. (2015)
$Cl + CH_3I \rightarrow CH_2I + HCl$	2.9×10^{-11}	1000	Burkholder et al. (2015)
$IO + DMS \rightarrow SO_2* + I$	3.2×10^{-13}	925	Saiz-Lopez et al. (2015)
$CH_2I + O_2 \rightarrow CH_2O + IO$	4.0×10^{-13}	—	Gravestock et al. (2010)
$IO + NO_3 \rightarrow OIO + NO_2$	9.0×10^{-12}	—	Saiz-Lopez et al. (2014)
$OIO + NO \rightarrow IO + NO_2$	1.1×10^{-12}	-542	Saiz-Lopez et al. (2014)
$IO + OIO \rightarrow I_2O_3$	1.5×10^{-10}	—	Badia et al. (2019)
$OIO + OIO \rightarrow I_2O_4$	1.5×10^{-10}	—	Badia et al. (2019)
$IO + Br \rightarrow I + BrO$	2.49×10^{-11}	—	Saiz-Lopez et al. (2014)
$I + IONO_2 \rightarrow I_2 + NO_3$	9.1×10^{-11}	-146	Saiz-Lopez et al. (2014)
$IO + CH_3O_2 \rightarrow CH_2O + I + HO_2$	2.0×10^{-12}	—	Saiz-Lopez et al. (2014)
$IO + ClO \rightarrow ICl + O_2$	9.4×10^{-13}	-280	Saiz-Lopez et al. (2014)
$IO + O_3 \rightarrow OIO + O_2$	3.6×10^{-16}	—	Saiz-Lopez et al. (2014)
$IO + OH \rightarrow HO_2 + I$	1.0×10^{-10}	—	Saiz-Lopez et al. (2014)
$HI + NO_3 \rightarrow I + HNO_3$	1.3×10^{-12}	1830	Saiz-Lopez et al. (2014)
$I_2O_2 + M \rightarrow OIO + I + M$	2.5×10^{14}	9770	Ordóñez et al. (2012)
$I_2O_2 + M \rightarrow IO + IO + M$	1.0×10^{12}	9770	Ordóñez et al. (2012)
$I_2O_4 + M \rightarrow OIO + OIO + M$	3.8×10^{-2}	—	Badia et al. (2019)

	$k_0=3.0 \times 10^{-31}$	1.0	Burkholder et al. (2015)
$I + NO_2 + M \rightarrow INO_2 + M$	$k_0=3.0 \times 10^{-31}$	1.0	Burkholder et al. (2015)
	$k_\infty=6.6 \times 10^{-11}$	0	
$INO_2 + M \rightarrow I + NO_2 + M$	9.94×10^{17}	11859	Badia et al. (2019)
$IO + NO_2 + M \rightarrow IONO_2 + M$	$k_0=7.5 \times 10^{-31}$	3.5	Burkholder et al. (2015)
	$k_\infty=7.6 \times 10^{-12}$	1.5	
$IONO_2 + M \rightarrow IO + NO_2 + M$	$k_0=5.0 \times 10^{-28}$	14120	Burkholder et al. (2015)
	$k_\infty=1.9 \times 10^{-7}$	2.5	
$I + NO + M \rightarrow INO + M$	$k_0=1.8 \times 10^{-32}$	1	Burkholder et al. (2015)
	$k_\infty=1.7 \times 10^{-11}$	0	

Part 2: Photochemical reactions

Chemical reaction	Method	Reference
$CH_3I + h\nu \rightarrow CH_3 + I$	Look-up table	Burkholder et al. (2015)
$CH_2I_2 + h\nu \rightarrow CH_2I + I$	Look-up table	Burkholder et al. (2015)
$I_2 + h\nu \rightarrow I + I$	Look-up table	Burkholder et al. (2015)
$IO + h\nu \rightarrow I + O$	Look-up table	Burkholder et al. (2015)
$OIO + h\nu \rightarrow I + O_2$	Look-up table	Burkholder et al. (2015)
$INO + h\nu \rightarrow I + NO$	Look-up table	Burkholder et al. (2015)
$INO_2 + h\nu \rightarrow I + NO_2$	Look-up table	Burkholder et al. (2015)
$IONO_2 + h\nu \rightarrow I + NO_3$	Look-up table	Burkholder et al. (2015)
$HOI + h\nu \rightarrow I + OH$	Look-up table	Burkholder et al. (2015)
$HI + h\nu \rightarrow I + H$	Look-up table	Burkholder et al. (2015)
$I_2O_2 + h\nu \rightarrow I + OIO$	Look-up table	Davis et al. (1996)
$I_2O_3 + h\nu \rightarrow IO + OIO$	Look-up table	Davis et al. (1996)
$I_2O_4 + h\nu \rightarrow OIO + OIO$	Look-up table	Davis et al. (1996)
$IBr + h\nu \rightarrow I + Br$	Look-up table	Burkholder et al. (2015)
$ICl + h\nu \rightarrow I + Cl$	Look-up table	Burkholder et al. (2015)
$CH_2ICl + h\nu \rightarrow I + Cl$	Look-up table	Burkholder et al. (2015)
$CH_2IBr + h\nu \rightarrow I + Br$	Look-up table	Burkholder et al. (2015)

Part 3: Heterogeneous chemical reactions on tropospheric cloud ice.

Chemical reaction	Reactive uptake coefficient [unitless]	Reference
$HOI + HI \rightarrow I_2 + H_2O$	$\gamma = 0.12$	Saiz-Lopez et al. (2015)
$HOI + HCl \rightarrow ICl + H_2O$	$\gamma = 0.12$	Saiz-Lopez et al. (2015)
$HOI + HBr \rightarrow IBr + H_2O$	$\gamma = 0.12$	Saiz-Lopez et al. (2015)
$IONO_2 + (H_2O) \rightarrow HOI + HNO_3$	$\gamma = 0.1$	Saiz-Lopez et al. (2015)

A-factor: the pre-exponential factor;

E$_a$: the activation energy;

R: the universal gas constant;

* SO$_2$ instead of DMSO is used (DMSO is absent in SOCOL-AERv2-I);

k_0: Low-pressure limit($cm^6 molecule^{-2}s^{-1}$);

k_∞:High-pressure limit ($cm^3 molecule^{-1}s^{-1}$)

We briefly review SOCOL's chlorine and bromine reactions because of their interaction with iodine chemistry. Apart from reactions involving iodine, there are about 100 gas-phase and 11 heterogeneous reactions on sulfates and polar stratospheric clouds (PSCs) for chlorine species and about 50 gas-phase and 4 heterogeneous reactions on sulfates and polar stratospheric clouds (PSCs) for bromine species. The total gas-phase chlorine (Cl_{tot}) and bromine (Br_{tot}) in the current version of the model are:

$Cl_{tot} = ClO + Cl + 2 \times Cl_2 + ClNO_3 + HOCl + HCl + 2 \times Cl_2O_2 + BrCl + 3 \times CFC-11 + 2 \times CFC-12 + 3 \times CFC-113 + 2 \times CFC-114 + CFC-115 + 4 \times CCl_4 + 3 \times CH_3CCl_3 + HCFC-22 + 2 \times HCFC-141B + HCFC-142B + H-1211 + CH_3Cl + 2 \times HCFC-21 + 2 \times HCFC-123 + HCFC-31 + ICl + CH_2ICl$ and

$Br_{tot} = Br + BrO + 2 \times Br_2 + BrCl + BrNO_3 + HBr + 2 \times CH_2Br_2 + CH_3Br + CBrF_3 + 3 \times CHBr_3 + HOBr + H-1301 + H-1211 + 2 \times H-2402 + IBr + CH_2IBr$.

Similar to the iodine schemes in CAM-chem (Ordóñez et al., 2012) and GEOS-Chem (Sherwen et al., 2016a), we implemented the free molecular transfer approximation of McFiggans et al. (2000). This allows introducing the iodine scavenging and deposition on sea-salt and sulfate aerosols as well as effective ice-uptake (removal)/reactive ice-uptake (recycling) on a surface of tropospheric cloud ice crystals (Fernandez et al., 2014; Saiz-Lopez et al., 2014, 2015). The transfer coefficient (s^{-1}) is calculated as follows:

$$k = \frac{1}{4}\gamma\langle c \rangle A, \tag{4}$$

where γ is the effective/reactive uptake coefficient (see Table 3), A is the surface area density (in cm^2 cm^{-3}) of the particles on which the deposition occurs, $\langle c \rangle = (8RT/\pi M)^{1/2}$ is the mean thermal molecular speed (in cm s^{-1}) of molecules with molar mass M (in Kg mol^{-1}) at absolute temperature T (in K), and R = 8.3145 J mol^{-1} K^{-1}.

In SOCOL-AERv2-I, sea-salt aerosols are prescribed by monthly means from observational data and aqueous sulfuric acid aerosols are calculated interactively; from both, surface area densities (SADs) are available. However, there is no readily available SAD for cloud ice in SOCOL-AERv2-I. Therefore, we calculate the effective radius R_{eff} (in mkm) of ice crystals following Heymsfield et al. (2014):

$$R_{eff} = \alpha exp(\beta T_c), \tag{5}$$

where T_c is the temperature (in C^o), $\alpha = 154.2$ and $\beta = 0.0152$ for $-56C^o < T < 0C^o$; $\alpha = 4.5872 \times 10^4$ and $\beta = 0.117$ for $-71C^o < T < -56C^o$; $\alpha = 41.65$ and $\beta = 0.0184$ for $-85C^o < T < -71C^o$. Following Holmes et al. (2019), the SAD for ice particles (in cm^2 cm^{-3}) is calculated from (R_{eff}) as follows:

$$SAD_{ice} = 6.75 \times IWC/(\rho R_{eff}), \tag{6}$$

where ρ is the density of ice (9.167×10^{-4} kg cm^{-3}) and IWC is the ice water content, i.e. the mass of ice per volume of air in the cloud (in kg cm^{-3}).

Since the timescale of the physical process of removing/recycling of iodine is shorter than the model time step (2 hrs), using an explicit integration scheme may result in excessive removal/recycling of iodine species leading to errors (such as negative concentrations). To avoid this, we decided to implement a simple implicit scheme:

$$C_1 = C_0/(1 + K \times \Delta t) \tag{7}$$

Where: C_0 - the initial concentration; K – transfer coefficient; C_1 – the final concentration; Δt - model time step for chemistry. This scheme avoids producing negative C_1.

As effective uptake coefficients (γ), we applied $\gamma_{IONO_2} = 0.01$, $\gamma_{INO_2} = 0.02$, $\gamma_{HOI} = 0.06$, $\gamma_{I_2O_2} = \gamma_{I_2O_3} = \gamma_{I_2O_4} = 0.01$ to model an effective uptake and removing of iodine species on sea-salt aerosols (Ordóñez et al., 2012).

Since γ's for sulfate aerosols are currently unknown and if consider effective uptake on sulfate aerosols with the same gamma as for sea-salt aerosols we would obtain modeled I_y values with a large bias (X %) against observations, for sulfate particles, γ's for sea-salt aerosols in SOCOL-AERv2-I were divided by 100 (as the amount of iodine to be removed on tropospheric sulfate aerosols is assumed to be 100 less than for sea-salt), which brought the iodine from SOCOL-AERv2-I to be closer to available observations. For effective ice-uptake of iodine, γ's are taken to be the same as in CAM-chem (Saiz-Lopez et al., 2014): $\gamma_{HOI} = 0.0003$; $\gamma_{IONO_2} = 0.005$; $\gamma_{HI} = 0.02$. The removal on all presented surfaces is operated only within the troposphere (it is confined by the tropopause height). It must be mentioned that the values of effective uptake coefficients for iodine species for

240   different types of surfaces are highly uncertain (Saiz-Lopez et al., 2014). It is worth saying that we only consider the deposition on sea-salt and sulfate aerosols and did not implement any heterogeneous recycling of iodine species on sea-salt aerosols like those described in Vogt et al. (1996, 1999),Ordóñez et al. (2012), Saiz-Lopez et al. (2014), and Tham et al. (2021). It should be noted that the lack of recycling on sea-salt aerosols may affect the I_y burden and the amount of stratospheric iodine injection. Yet, it requires additional study to estimate it quantitatively.

245   In the heterogeneous recycling mechanism on ice, reactive uptake coefficients for cloud ice are taken as follows: $\gamma_{HOI} = 0.12$; $\gamma_{IONO_2} = 0.1$ (see Saiz-Lopez et al. (2015) supplements). Transfer coefficients for heterogeneous reactions (see Table 3) are also calculated by free molecular transfer approximation (McFiggans et al., 2000) but using reactive uptake coefficients. The reactive ice-uptake and recycling of HOI and $IONO_2$ is applied in SOCOL-AERv2-I after effective ice-uptake and removing of HOI, $IONO_2$, and HI. The sequence of removing/recycling processes is unclear but the chosen sequence shows reasonable

250 results. Also, it should be noted here that there is no evidence of reactive uptake and recycling of iodine species in liquid clouds, and in our scheme, we use it only for ice crystals as was done by Saiz-Lopez et al. (2015).

2.3   Conducted experiments

To evaluate the iodine chemistry scheme of SOCOL-AERv2-I as well as to estimate the influence of iodine chemistry on ozone we designed and carried out three transient numerical experiments. The first one is the control experiment where iodine emis-

255 sions are set to zero. For the second experiment ($1 \times$ iodine), we applied a basic configuration with the present-day iodine emissions. These experiments are used to evaluate the veracity of iodine in SOCOL-AERv2-I and to estimate the influence of iodine chemistry on present-day ozone climatology.

To assess whether the potential intensification of iodine emissions in the future will have a tangible effect on the ozone layer, we designed a sensitivity experiment (to verify the sensitivity of ozone to iodine) in which all iodine emissions are doubled

260 to present-day emissions ($2 \times$ iodine). In essence, it could be assumed as a worst-case scenario compared to the present-day emissions that might become closer to reality by the middle of this century if the rise of emissions presented by Cuevas et al. (2018) and Legrand et al. (2018) continued despite no dramatic forecast of iodine emission's evolution was made by Iglesias-Suarez et al. (2020). The iodine content in the future is also difficult to predict due to a huge discrepancy between scenarios for the future evolution of iodine precursors like tropospheric ozone (Archibald et al., 2020) and SST (Taylor et al., 2012).

265 Albeit, it should be said that in our study this assumption was used only to verify the sensitivity of ozone to iodine chemistry. The sensitivity of ozone to the increase of the iodine emissions was characterized by comparing experiments with $2 \times$ and $1 \times$ loading of iodine. All experiments were run for the 1990-2009 period including the 10-year spin-up (1990-1999) from the initial conditions that is necessary for iodine to reach the quasi-equilibrium state. The spin-up period was excluded from further analysis. Each experiment consists of 10 ensemble members with a one-month perturbation of initial CO_2 concentration to get

270 10 different atmospheric realizations and to calculate the statistical significance of the iodine influence on ozone using the t-Student test. The summary of the experimental set-up can be found in Table 4.

Table 4: The experiments with SOCOL-AERv2-I

Name of experiment	Experiment description	Period of simulation and spin-up
$0 \times$ iodine	Control run	1990-2009
	(10 ensemble members)	(1990-1999 spin-up)
$1 \times$ iodine	Present-day emissions	1990-2009
	(10 ensemble members)	(1990-1999 spin-up)
$2 \times$ iodine	Doubled emissions	1990-2009
	(10 ensemble members)	(1990-1999 spin-up)

3 Results of simulation

3.1 Evaluation of the iodine from SOCOL-AERv2-I against CAM-chem and observations

The total gas-phase inorganic I_y both $2 \times$ iodine and $1 \times$ iodine experiments of SOCOL-AERv2-I averaged over tropics [20°N - 20°S], for the 2000-2009 period and 10 ensemble members is presented in Figure 2.
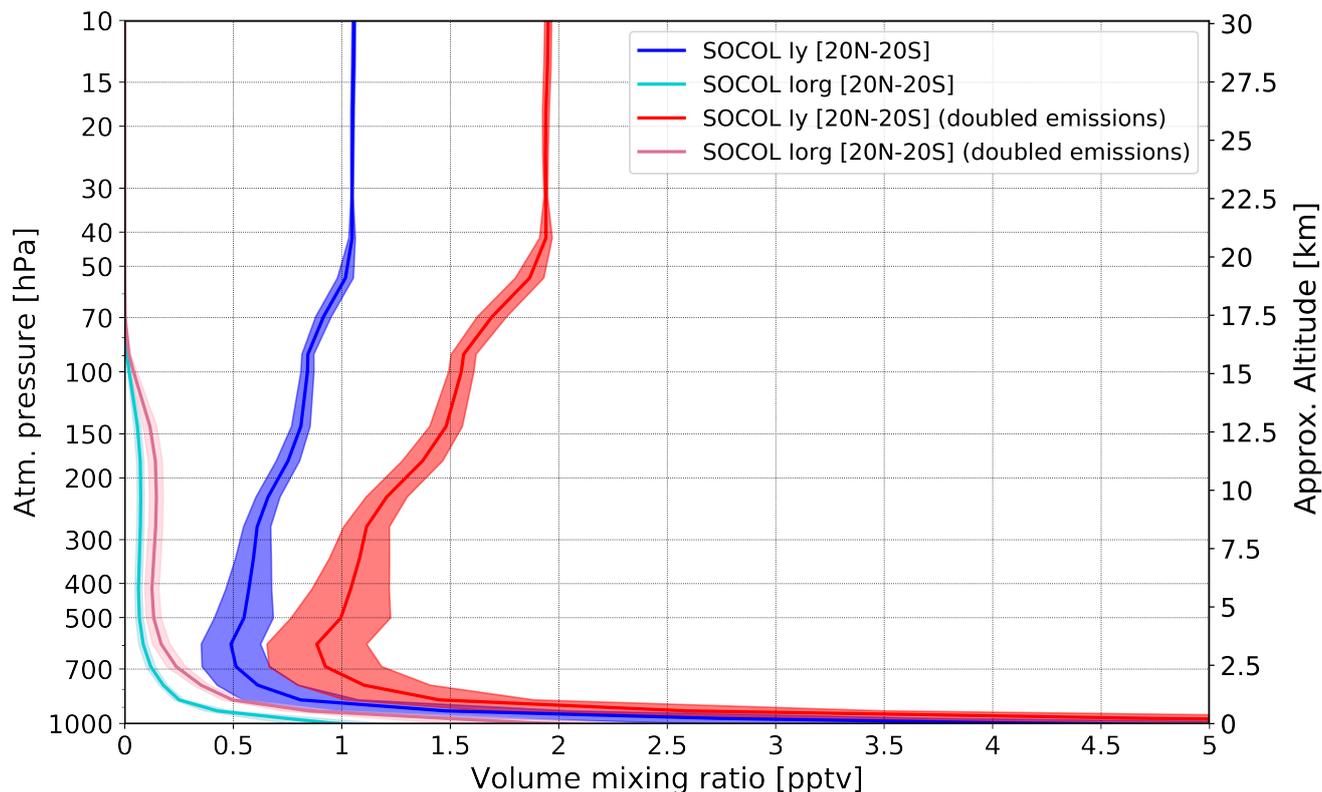
Figure 2. Modeled vertical distribution of total organic (I_{org}) and inorganic (I_y) gas-phase iodine simulated with SOCOL-AERv2-I averaged over tropics [20°N - 20°S], for 2000-2009 period and 10 ensemble members. Red curve: I_y from the experiment 2 $\times$ iodine. Blue curve: I_y from the experiment 1 $\times$ iodine. Light red and blue curves: I_{org} from 2 $\times$ iodine and 1 $\times$ iodine experiments, correspondingly. Shadings represent a standard deviation of tropical iodine [20°N - 20°S].

The I_y was calculated as a sum of inorganic iodine compounds presented in the SOCOL-AERv2-I's iodine scheme: I_y = IO + I + OIO + HOI + 2 $\times$ I_2 + HI + INO + INO_2 + 2 $\times$ (I_2O_2 + I_2O_3 + I_2O_4) + ICl + IBr + $IONO_2$ + CH_2I. I_{org} is calculated as 280 a sum of all organic compounds in SOCOL-AERv2-I: I_{org} = CH_3I + 2 $\times$ CH_2I_2 + CH_2ICl + CH_2IBr. The standard deviation of iodine between ensemble members is found to be less than 1%. In the lower troposphere, the I_y is rapidly dropping with altitude until about 600 hPa following the washout that is most effective at this layer. In the upper troposphere (above 200 hPa), I_y increases after the initiation of the recycling heterogeneous mechanism on ice that works at these altitudes at tropics because the availability of cloud ice is essential. The recycling on cloud ice mostly defines the amount of inorganic iodine 285 injected into the stratosphere because it competes with the washout of reservoir species by converting reservoirs into species with lower washout rates and thus increasing the residence lifetime. The stratospheric I_y shows an increase until about 50 hPa and then stays constant because there is no deposition of iodine above this layer. The simulated stratospheric I_y by SOCOL-AER2-I agrees well with the results of the CAM-chem model in the lowermost stratosphere showing about 0.75-0.8 pptv of I_y,

however, it becomes higher in the middle stratosphere than in Saiz-Lopez et al. (2015). We suggest that it might have resulted
290 from model non-conservative transport scheme and dynamics, for example, the deep tropical convection cells over the area of
iodine production that overcomes the deposition velocity enhancing the stratospheric iodine loading. Higher values of I_y in the
stratosphere relative to the upper and middle troposphere can be also explained by the rapid tropospheric sinks and relatively
slow transport of I_y into the troposphere. A hard upper border in SOCOL-AER2-I that prevents chemical species from going
through it also might impact the profile. Nevertheless, the stratospheric I_y abundance calculated with SOCOL-AER2-I does
295 not exceed 1.05 pptv and corresponding well to the estimation given by Solomon et al. (1994), although is slightly larger than
the most recent assessment from (WMO, 2018) (0.8 pptv I_y).
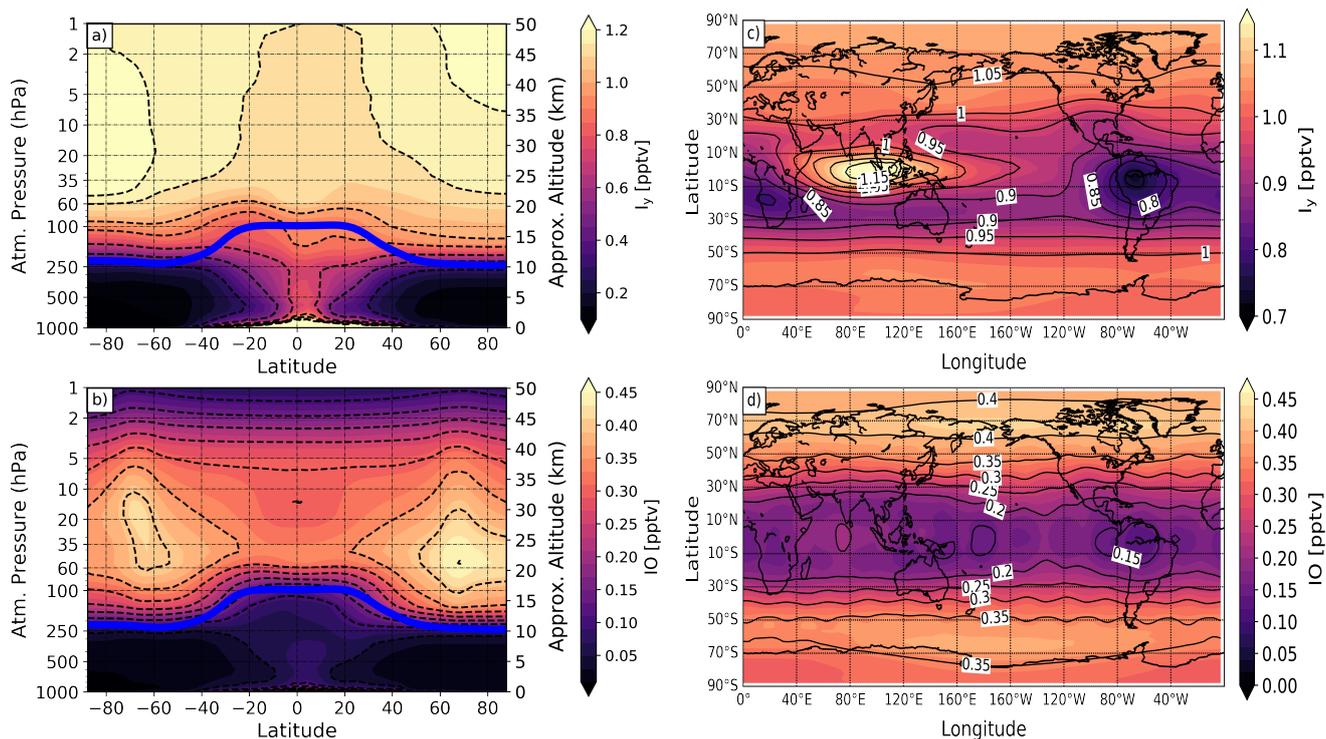
Figure 3. Modeled vertical distribution and global map of total inorganic gas-phase iodine (I_y) and iodine monoxide (IO) simulated with
SOCOL-AERv2-I from the experiment with present-day iodine emissions (1 × iodine), averaged for 2000-2009 period and 10 ensemble
members. (a+b) zonal-mean vertical distributions of I_y and IO. (c+d) global maps of I_y and IO averaged for 100-70 hPa region. Blue solid
line in (a) and (b): annual mean tropopause height.

Figure 3 presents the vertical distributions of I_y and IO at all latitudes and global maps of I_y and IO averaged for the lower
stratosphere (100-70 hPa). I_y and IO have the highest mixing ratio at the polar regions of the stratosphere due to transport

16

300   carried out by Brewer–Dobson circulation (BDC). The larger stratospheric values of IO at high latitudes are also related to the higher O_3 abundance at those locations. At the tropics, there are two pronounced areas with a higher (over Indian ocean) and with a lower (over South America) I_y mixing ratio as depicted in Figure 3 c). Their formation might have resulted from different convection patterns (weaker/stronger) over these areas. Also, the area with a higher stratospheric I_y burden is located right over the region with higher surface emissions of HOI/I_2 (see Figure 1). In the troposphere, the iodine level is decreasing

305   toward the poles and far from the iodine source regions. The iodine distribution demonstrates the highest mixing ratio of iodine in the lower stratosphere over middle-to-high latitudes with a maximum I_y of more than 1.15 pptv in the polar region of the Northern hemisphere and about 1 pptv in the Southern hemisphere. The IO has two maximums of about 0.4 pptv in the lower-to-middle stratosphere and high latitudes. Also, note that IO decreases at higher levels of the stratosphere exhibiting more than five times less abundance than in the lower stratosphere, which might result from decreasing the efficiency of O_3-I reactions.

310   We compared the mixing ratio of iodine compounds with some of the local measurements mentioned above. The modeled reactive IO over Scandinavia (70^oN; 20^oE) in March is > 0.45 pptv at 17 km (monthly-mean value) that is in agreement with IO simulated with box-model that was partly initialized with the IO retrieved by balloon flights (a day-time concentration $\sim$ 0.65 pptv at 17 km) (Pundt et al., 1998). Yet, the balloon-borne measured upper limit of IO mixing ratio is 0.2 pptv (Pundt et al., 1998) that is more than 2 time lower than IO mixing ratio simulated with SOCOL-AER2-I. SOCOL-AER2-I also captures well

315   the I_y estimated by box-model (Pundt et al., 1998) showing a mixing ratio of 1-1.1 pptv. Also, IO simulated with SOCOL-AERv2-I is corresponding well with DOAS measurements over Spitsbergen island (79^oN; 12^oE) in March (Wittrock et al., 2000) showing > 0.48 pptv in the lower stratosphere. Farther, we compare the iodine monoxide (IO) obtained by SOCOL-AER2-I with the one from the CAM-chem model and the recent aircraft observations with AMAX-DOAS conducted during the TORERO and CONTRAST campaign (Volkamer et al., 2015; Pan et al., 2017). The results are shown in Figure 4.
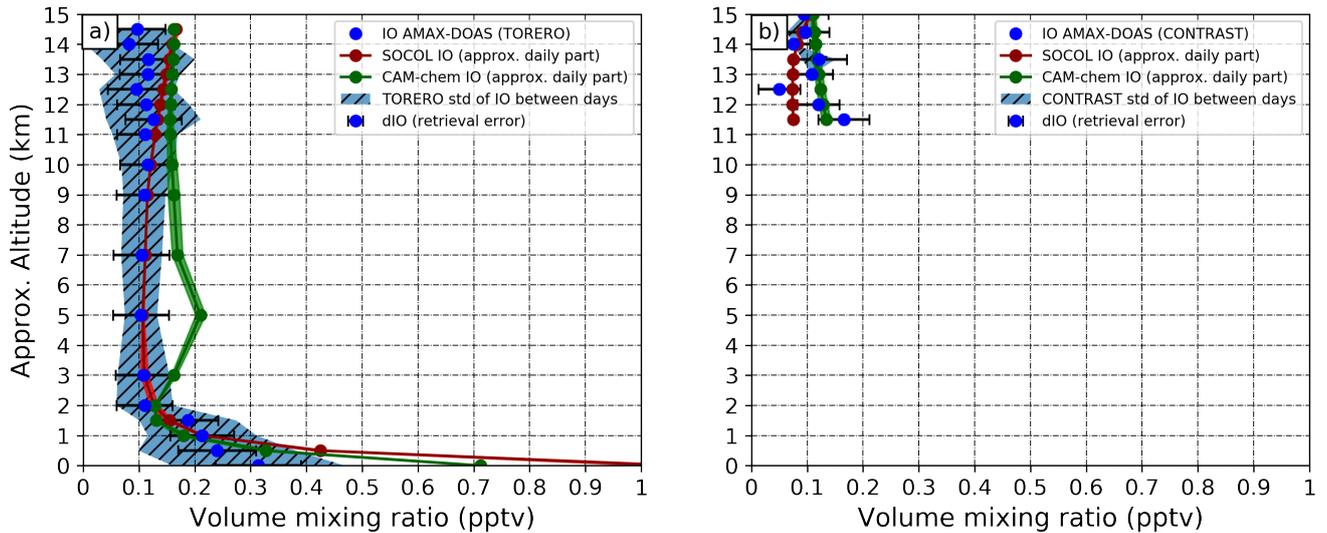
Figure 4. January/February averages of modeled and observed IO in the tropical troposphere [15°N-15°S] for (a) the TORERO campaign from Costa Rica (Jan./Feb. 2012, 10°N-40°S, 250°E-285°E), and (b) the CONTRAST campaign from Guam (Jan./Feb. 2014, 40°N-15°S, 115°E-175°E). Red line: IO from SOCOL-AERv2-I. Green line: IO from CAM-chem. Blue dots: IO observed by AMAX-DOAS. Shadings: IO standard deviations of all modeled/measured IO during the January-February period.

320   We compare the observed and measured IO only over the tropics [15°N-15°S] as extratropical measurements from both campaigns are scarcer and the comparison will be biased. Modeled IO in Figure 4 has been obtained by doubling monthly averaged IO that is fair to do for tropics as during nighttime the IO concentration is negligible. Also, the observations are given as so-called footprints to get profiles for each day; they were around-averaged for certain altitudes designated in Figure 4 as blue points. The around-averaged values for Figure 4 are obtained by averaging all measurements taken in the nearby altitude

325 ranges. The IO from both models is sampled at the same altitudes as measurements to conduct an equitable comparison. It should be noted that from the CONTRAST campaign, tropical IO measurements in the upper troposphere are only available. Both SOCOL-AERv2-I and CAM-chem overestimate observations from the TORERO campaign at near-surface levels. The sharp decrease of observed and modeled IO from both models goes similarly until 2 km showing compatible IO mixing ratios. At 5 km, CAM-chem shows a maximum IO mixing ratio of about 0.2 pptv that is not seen in SOCOL-AERv2-I and

330 observations. CAM-chem generally overestimates SOCOL-AERv2-I and observations during the TORERO campaign up to about 11-12 km. After 11 km, both models overestimate the mean of observed IO from the TORERO campaign but in general staying within the uncertainty of observations. The increase in modeled IO after 12 km might follow the recycling activity on ice, albeit it is not seen over the region of the CONTRAST campaign. IO from both models is generally compatible with IO measurements during the CONTRAST campaign showing the IO mixing ratio of about 0.1-0.15 pptv.

335

Besides, we made a comparison of modeled I_y from SOCOL-AERv2-I and CAM-chem models with the I_y derived from IO/I_y ratio modeled with the University of Colorado (CU) chemical box-model constrained by measured temperature, pressure, chemical concentrations, particle size distributions, and photolysis frequencies. The uncertainty in derived I_y is estimated as 30% of the IO/I_y ratio including errors in the calibration of in-situ and remote sensing data and accounting for differences in the spatial scales (Wang et al., 2015; Koenig et al., 2017). IO was taken as an average of IO fields measured with AMAX-DOAS during both TORERO and CONTRAST campaigns (Volkamer et al., 2015; Pan et al., 2017; Koenig et al., 2020). Thus, the inferred I_y is based on the measured IO and modeled IO/I_y. The result of this comparison is illustrated in Figure 5.
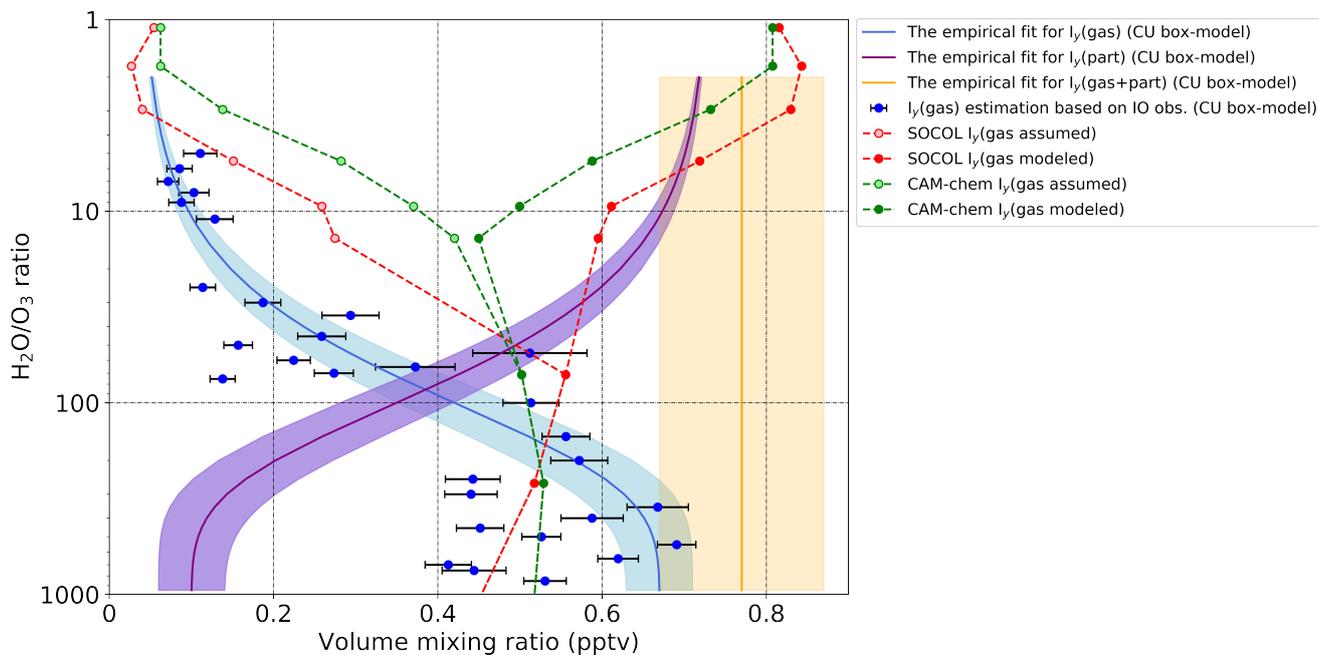
Figure 5. Total gas-phase I_y modeled with SOCOL-AERv2-I and CAM-chem as well as estimated by CU chemical box-model based on AMAX-DOAS IO observations in the upper troposphere and lowermost stratosphere. All model data and observations are taken only for the region of TORERO [10°N-40°S, 250°E-285°E] and CONTRAST measurements [40°N-15°S, 115°E-175°E]. Red and green solid and dashed lines: gas-phase I_y simulated with SOCOL-AERv2-I and CAM-chem averaged for the January-February period. Light red and light green dashed lines: assumed gas-phase I_y simulated with SOCOL-AERv2-I and CAM-chem excluding approx. iodine in the particulate phase. Blue dots: gas-phase I_y modeled by the University of Colorado (CU) chemical box-model. Black error bars: the uncertainty in I_y modeled by the CU box-model. Blue, purple, and orange solid lines represent the empirical fit for gas-phase I_y (gas), particulate I_y (part) and total I_y (gas+part), correspondingly. Shadings represent the uncertainty in the empirical fit.

Data were plotted with respect to the H_2O/O_3 ratio as it is a good indicator to distinguish the upper troposphere (UT) air enriched in water vapor from the dehydrated air in the lower stratosphere as proposed by Koenig et al. (2020). To make CU box-model data clearer they were thinned out by averaging the data every 50 units of H_2O/O_3 ratio between 1000 and 100 of

H$_2$O/O$_3$ ratio; every 5 units between 10 and 1; and every 1 unit between 10 and 1. The blue empirical fit is to a subset of the blue dots, that the orange line is based on I$_y$ (gas) and I$_y$ (part) data in the upper troposphere, and the purple line is derived under the assumption of conversion. Equations to calculate empirical fit lines for experimental data can be found here (see equation 2, 4, and 5 in Koenig et al. (2020) supplements).

350   Below the H$_2$O/O$_3$ ratio $\sim$70, both models well-capture the I$_y$ estimated from observations. Higher up, the red and green dashed lines represent the gas-phase I$_y$ that is simulated with both models. Because the particulate iodine is not considered in these models, the total inorganic I$_y$ in SOCOL-AERv2-I and CAM-chem presented here is only in the gas-phase. The light red and green lines are the assumed gas-phase I$_y$ if the estimated particulate iodine is excluded from the modeled I$_y$. To exclude the unknown particulate iodine, the modeled gas-phase I$_y$ was subtracted from the 0.87 pptv of iodine that is empirical total

355   I$_y$ plus uncertainty of observations (0.1 pptv) (see the orange solid line and its uncertainty in Figure 5). Such an approach can show what would be the approximate modeled gas-phase I$_y$ if the iodine in the particulate phase was presented in models. It is seen that after the level of H$_2$O/O$_3$ ratio $\sim$ 70, the gas-phase I$_y$ estimated from measurements rapidly decreases and reaches the value of about 0.1 pptv at the approximate altitude of the lowermost stratosphere (H$_2$O/O$_3$ ratio < 10). After excluding the estimated particulate iodine, the assumed modeled gas-phase I$_y$ becomes very close to the one from the CU box-model.

360   It bears mentioning that there is evidence that a certain part of gas-phase iodine undergoes partitioning to aerosol in the stratosphere. This mechanism is not fully understood due to a lack of measurements. Note that the approach used here is different from the simplified parameterization of IPART in CAM-Chem (Koenig et al., 2020). The assumption that the overestimation of modeled gas-phase I$_y$ against observations is because of an absence of iodine in the particulate phase is reasonable as it is seen in Figure 5. In this work, we do not consider particulate iodine for the analysis of ozone loss as it is out of the scope of the

365   paper. Here, we assume that the total stratospheric I$_y$ is only in the gas-phase. Nevertheless, the total amount of iodine obtained with SOCOL-AERv2-I is in good agreement with other estimates and observations and can be used in further analysis of its effect on ozone.

3.2   Iodine chemistry effect on present-day ozone climatology

We estimate the iodine effect on present-day ozone climatology by comparing the experiment with a single loading of iodine

370   (1 $\times$ iodine), and the control experiment neglecting iodine chemistry (0 $\times$ iodine). The contribution of iodine chemistry to present-day ozone climatology estimated by the SOCOL-AERv2-I is presented in Figure 6.
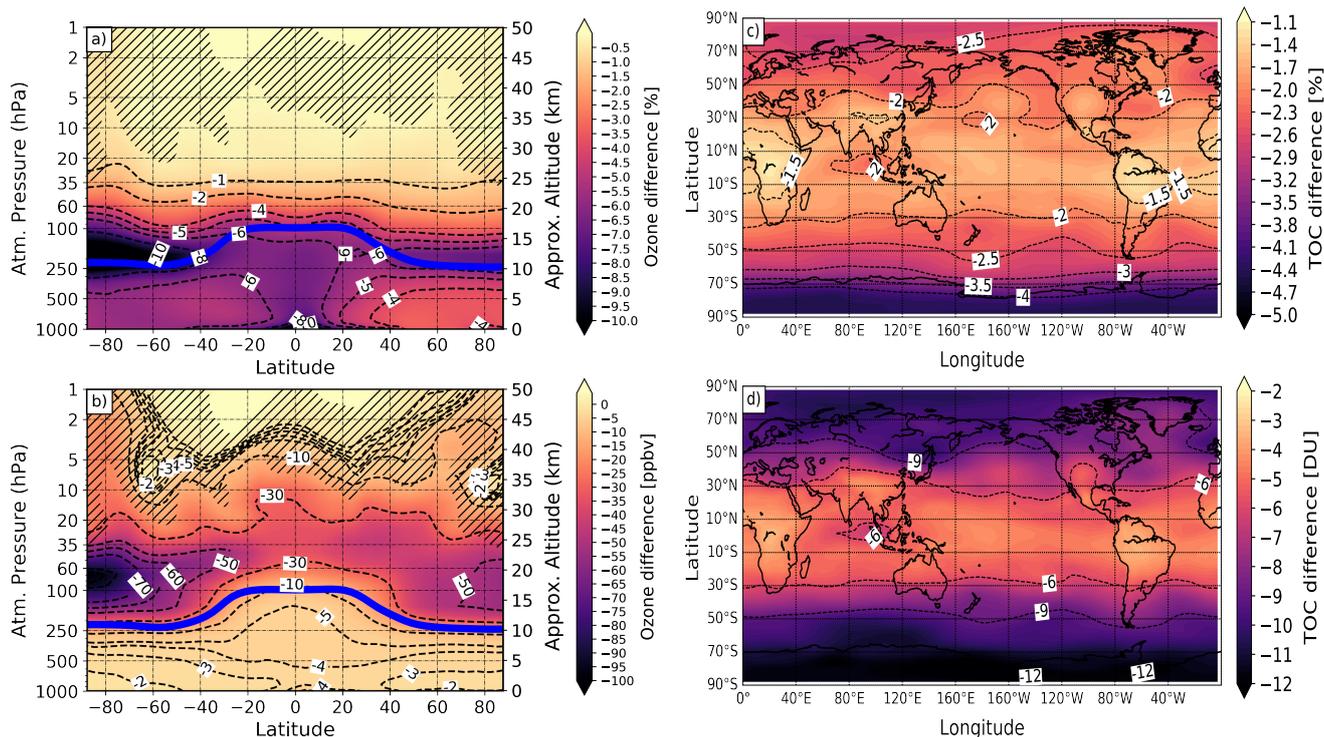
Figure 6. Modeled effect of iodine chemistry on annual-mean ozone climatology averaged for 2000-2009 period and 10 ensemble members. (a+c) Ozone changes of the case with present-day iodine emissions (1 × iodine) relative to the control run (0 × iodine), presented as zonal mean ozone mixing ratios and total ozone columns (TOC) in percent. (b+d) Corresponding absolute ozone changes in parts per billion by volume (ppbv) and Dobson units (DU), respectively. Blue solid line in (a) and (b): annual mean tropopause height. Hatching marks regions with iodine effect on ozone having a confidence level less than 95%.

The relative and absolute responses of ozone to iodine chemistry activation are shown for both ozone mixing ratio and total ozone column (TOC). The relative iodine effect on ozone is calculated as follows: ((EXP-REF)/REF)*100, where EXP is the ozone from the experiment with 1 × loading of iodine and REF is the control run without iodine being included. The absolute

375   difference is simply defined as EXP-REF. The crisp iodine signal in ozone mixing ratio is observed in the lower stratosphere and intensifies over the polar regions where the effect of halogens is estimated to be higher (Chipperfield et al., 2018). The peak of ozone loss resides in the lower stratosphere over the high southern latitudes, where the ozone loss reaches about 10% or 100 ppbv. The hemispheric asymmetry of the effect over high latitudes might be caused not only by a difference in the IO_x mixing ratio but also in the mixing ratio of chlorine and bromine in active form (ClO and BrO) that in turn react with iodine.

380   The effectiveness of iodine also depends upon the coupling with chlorine and bromine chemistry intensifying their ozone depletion cycles in the lower stratosphere (see chemical reactions in Table 3). There is evidence that cross-cycles between bromine and chlorine are the dominant contribution to ozone reduction in the mid-latitudes and polar region (Fernandez et al.,

21

2017; Alejandro Barrera et al., 2020). The active iodine in the form of IO is also an effective reaction partner for the BrO+ClO as established by Read et al. (2008). Thompson et al. (2015) assumed that the interaction of IO with the BrO and ClO might be more effective over high latitudes because of their higher concentration in that region (Sioris et al., 2006).

To verify whether or not cross-reactions of iodine with bromine and chlorine largely contribute to the total iodine effect on ozone, we performed an additional experiment where we set the reaction coefficients of all chemical reactions of iodine with chlorine (I-Cl) and bromine (I-Br) to zero. The contribution of iodine chemistry to present-day ozone climatology excluding I-Cl and I-Br cross-reactions estimated by the SOCOL-AERv2-I is presented in Figure 7.
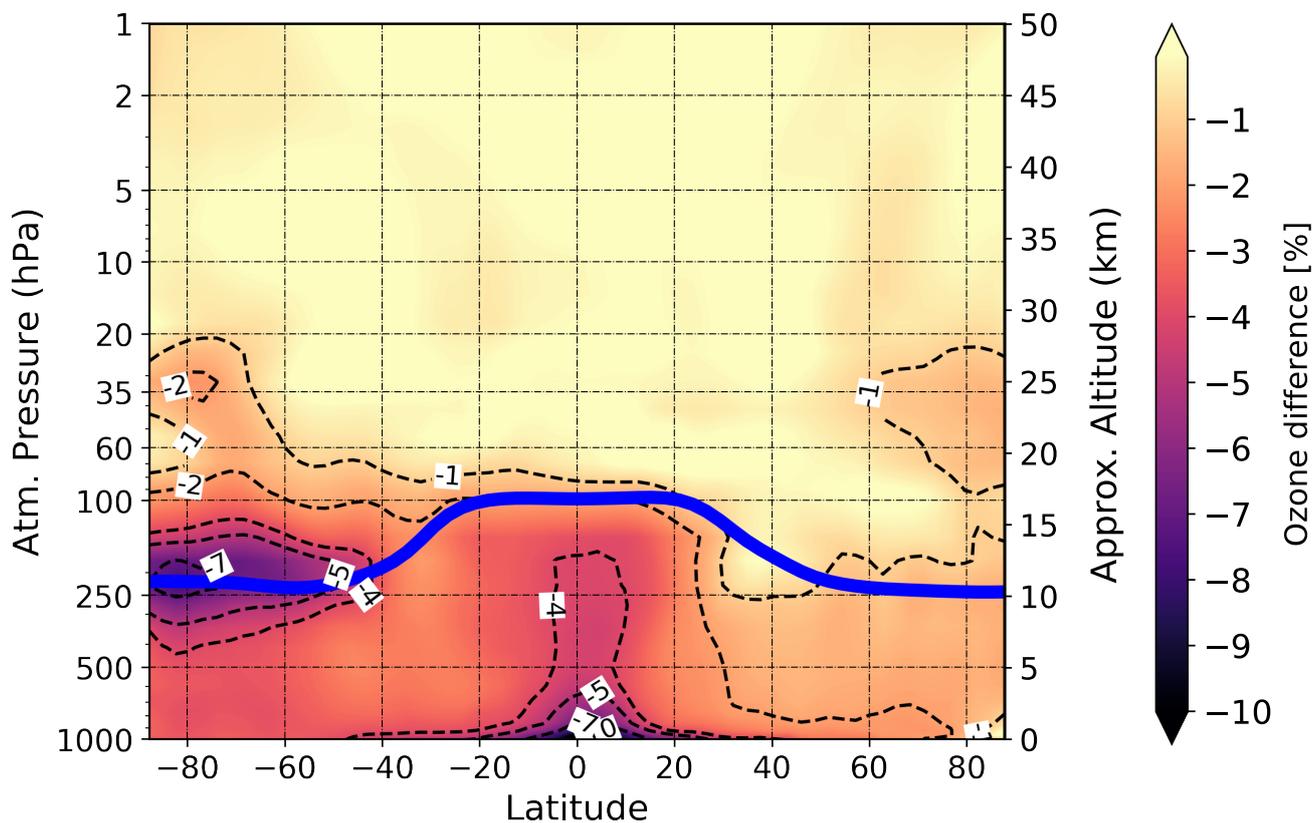
Figure 7. Modeled effect of iodine chemistry on annual-mean ozone climatology excluding I-Cl and I-Br cross-halogen reactions, averaged for 2000-2009 period. Presented ozone changes of the case with present-day iodine emissions (1 × iodine) relative to the control run (0 × iodine). Blue solid line: annual mean tropopause height.

Comparing Figure 6 a) and Figure 7, one can say that the inter-halogen cross-reactions are minor contributors to tropospheric ozone responsible only for about 20% of total iodine-induced ozone loss. However, in the lower stratosphere, the contribution of these cross-cycles is much higher, covering the 60-70% of total iodine effect on ozone in the Northern hemisphere. In the Southern hemisphere, the contribution is found to be less than ∼ 30%. Thus, our model suggests that cross-cycles of I with Cl

and Br might largely affect ozone and be responsible for more than a half of total iodine-induced ozone reduction in the lower
stratosphere that is agreed with Fernandez et al. (2017); Alejandro Barrera et al. (2020).

The iodine-mediated ozone loss in the tropical lower stratosphere ranging between 4–5% or 20 ppbv below 20 km. The
ozone destruction caused by iodine chemistry is not so pronounced over the tropics because the extremely low temperature in
the cold trap on the tropical tropopause resulted from adiabatic cooling is even lower than the temperature over high latitudes
at the same height making catalytic cycles less effective.

It is important to mention that the effects of iodine chemistry are confined mostly to the lower stratosphere and are greatly
decreasing from the middle to the upper stratosphere. The "glasses-like" iodine effect in the upper stratosphere similar to
the one of ClO_x - cycle (Zubov et al., 2013) is not observed. The IO_x-catalytic cycle is ineffective in the upper stratosphere
similarly to BrO_x-cycle despite the presence of atomic iodine up there in reasonable concentration. It might be because iodine
reservoirs are much more unstable than those of chlorine and, similarly to bromine, the iodine species in lower altitudes will
be more likely in active form (IO) than that of chlorine will be in form of ClO (Daniel et al., 1999). So, the probability of the
terminal reaction ClO+O is higher than those of IO+O or BrO+O in the upper stratosphere. It should be noted that SOCOL-
AERv2-I demonstrates the decrease of the IO mixing ratio in the upper stratosphere (see Figure 3 b)). Hence, the effect of
iodine chemistry on upper stratospheric ozone loss is negligibly small.

The tropospheric effect is $\sim$ 4-5 ppbv and maximizes over tropics where iodine sources are mostly emitted from the ocean
thanks to its higher temperature. About 6-8% of tropospheric ozone loss is comparable to what was reported by Sherwen et al.
(2016a) but where surface iodine emissions were a bit higher. It is also in agreement with an estimation made by Davis et al.
(1996). Tropospheric ozone loss in SOCOL-AERv2-I is a bit higher than in CAM-chem where the iodine-induced ozone loss
does not exceed 2-3 ppbv (Saiz-Lopez et al., 2014).

The total ozone column (TOC) is affected by iodine mostly over high latitudes (see c) and d) panels of Figure 6). The highest
impact of iodine on climatological TOC is over high latitudes of the Southern Hemisphere showing the TOC loss of about 4%
or 11-12 DU. Over the Northern Hemisphere, the iodine effect on TOC does not exceed 3%.

3.3   Ozone response to the increased iodine emissions

To estimate the consequences for ozone from the continuous increase of iodine emissions, we compare ozone from the exper-
iment with doubled emissions to that from the experiment with observed (or present-day) emissions. The results are shown in
Figure 8.
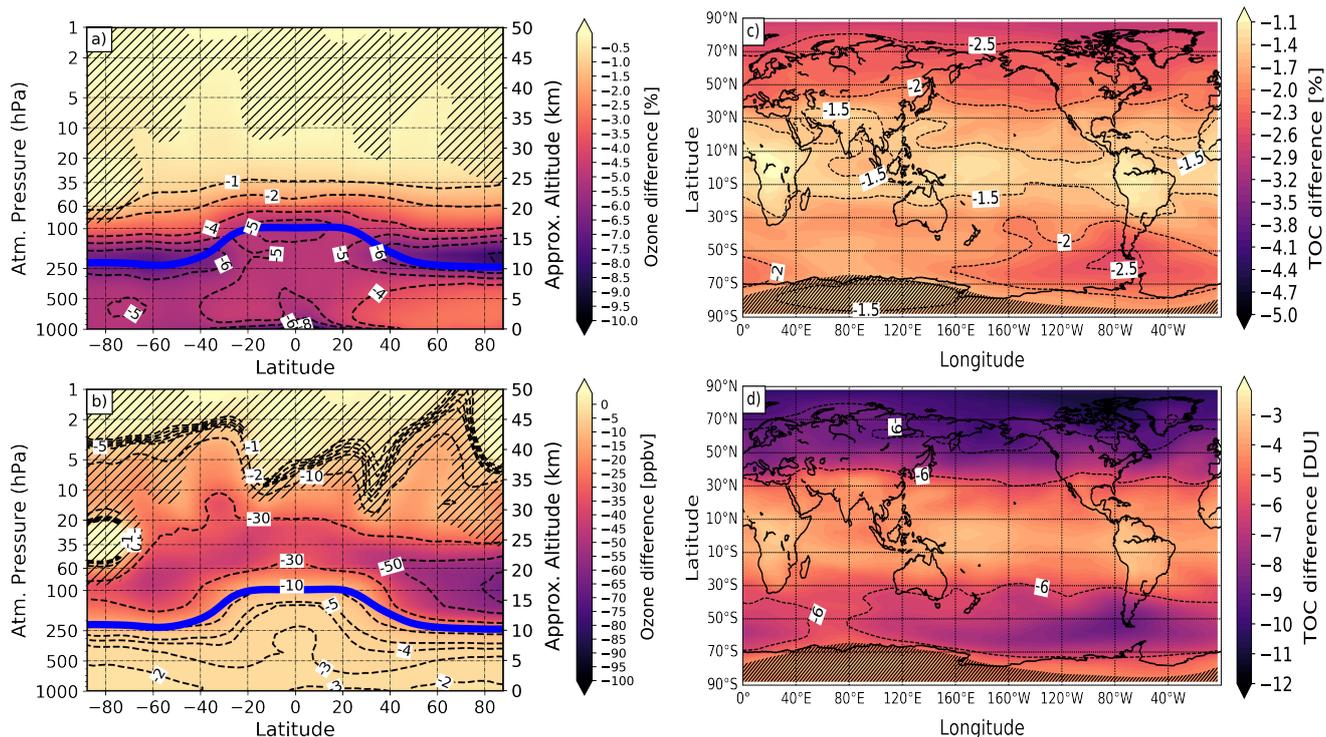
Figure 8. Modeled effect of 2-fold iodine chemistry on annual-mean ozone climatology averaged for 2000-2009 period and 10 ensemble members. (a+c) Ozone changes of the case with 2-fold iodine chemistry (2 × iodine) relative to present-day iodine emissions (1 × iodine) in percent. (b+d) Corresponding absolute ozone changes in parts per billion by volume (ppbv) and Dobson units (DU), respectively. Blue solid line in (a) and (b): annual mean tropopause height. Hatching marks regions with iodine effect on ozone having a confidence level less than 95%.

In this case, the EXP was taken to be the experiment with 2 × loading of iodine whereas the REF is the one with observed (1 ×) iodine emissions. In the troposphere, a 2-fold increase in emissions leads to the ozone loss of about 6-8% that is similar to what is seen in Figure 6. In the stratosphere, the contribution of additional iodine is different. The Southern hemispheric maximum is weakened and shifted to the middle latitude showing the ozone loss of up to 7% or 50 ppbv. The iodine con-
425   tribution to ozone loss in the northern polar lowermost stratosphere also shows a similar pattern and magnitude of the effect to climatological effect in Figure 6 showing about 50 ppb of ozone loss. For the Northern Hemisphere, the effect might be characterized as a linear-kind too and the intensification of ozone loss by a factor of 2 can be expected. The iodine-induced total column ozone loss would enhance by 2-3% following the 2-fold increase of iodine emissions.

430   Thus, we can expect that a 2-fold increase in iodine injection into the atmosphere would lead to a mostly linear increase of the ozone loss over the troposphere and lower stratosphere. The reason why we do not see the linearly changed effect over the

Southern Hemisphere is possibly related to the saturation effect when the ozone was almost destroyed even for smaller iodine loading. Hence, it can be predicted that the iodine effect on ozone in the lower atmosphere, if the assumed negative iodine scenario plays out in the future, would simply hinge on a factor of the increasing iodine injection into the atmosphere.

435 3.4 Ozone response to organic and inorganic iodine sources

We also address the effect of organic vs inorganic iodine sources on tropical ozone. To do this, we repeated the experiment with observed (or present-day) emissions twice setting either organic or inorganic surface emissions to zero. The results are shown in Figure 9.
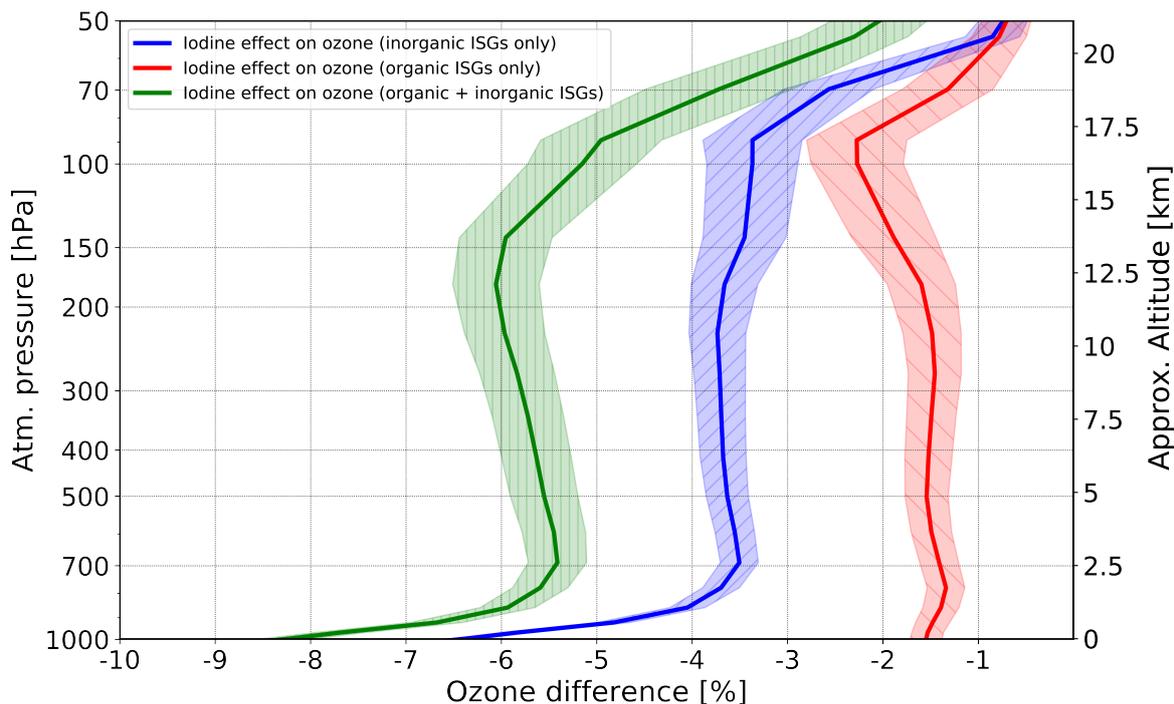
Figure 9. Modeled vertical profiles of O_3 reduction by iodine from organic, inorganic, and total surface emissions averaged over tropics [20^oN - 20^oS], for 2000-2009 period and 10 ensemble members. Red curve: difference in O_3 relative to the control run (0 × iodine), if organic iodine source gases are only considered; Blue curve: a % difference in O_3 relative to the control run (0 × iodine), if inorganic iodine source gases are only considered; Green curve: a % difference in O_3 relative to the control run (0 × iodine), if both, organic and inorganic iodine source gases are considered. Shadings represent a standard deviation of ensemble members. The results have a confidence level more or equal to 95%.

In the lower troposphere, the iodine from inorganic emissions is responsible for $\sim$ 75% of total iodine effect on ozone, and the contribution of iodine from organic sources is $\sim$ 25%, as expected (Koenig et al., 2020). In the upper troposphere and lower stratosphere, the ozone responses to iodine from both kinds of sources are closer but still, the impact of inorganic sources

prevails, i.e. $\sim 60\%$ and $\sim 40\%$, correspondingly. At 50 hPa, the contributions of iodine originating from organic and inorganic sources to total iodine-induced ozone reduction are compatible.

4 Discussion and conclusions

445   In this study, we describe the new version of the chemistry-climate model SOCOL-AERv2 improved with the addition of the iodine chemistry module. The iodine chemistry scheme in SOCOL-AERv2-I was developed based on up-to-date knowledge about atmospheric iodine. We performed a set of numerical experiments to test the fidelity of the developed iodine chemistry scheme and to estimate iodine contribution to ozone depletion. The model results show about 0.75 pptv of iodine in the lowermost tropical stratosphere in agreement with previous estimations Saiz-Lopez et al. (2015). A gradual increase of I_y up to 1.05

450   pptv in the stratosphere might be related to the dynamical features, the effect of tropospheric sinks and/or recycling, or the rigid upper border in the model atmosphere. The comparison of modeled and observed IO within the tropical troposphere showed that IO from SOCOL-AERv2-I is in a generally good agreement with AMAX-DOAS observations. The additional comparison of total gas-phase inorganic I_y with the values determined by the CU box-model based on AMAX-DOAS observations of IO showed that the model reproduces the I_y in the upper troposphere very well, while in the stratosphere, I_y is much overestimated

455   due to the absence of simulated iodine in the particulate phase. If the assumed particulate iodine was excluded from the modeled stratospheric I_y, SOCOL-AERv2-I corresponds well with I_y from the CU box-model. The simulation of particulate iodine is the subject for future studies as the mechanism of its formation is still not fully understood due to a lack of measurements.

The estimated contribution of iodine chemistry on the lower stratospheric ozone is higher than those discussed in Hossaini

460   et al. (2015) showing up to 10% of the lower stratospheric ozone loss driven by iodine chemistry. It should be noted that Hossaini et al. (2015) reported only 0.15 pptv of I_y injected into the stratosphere, which is more than five times less than in SOCOL-AERv2-I and CAM-chem. In the lower troposphere, the share of ozone loss induced by iodine originating only from inorganic sources is estimated to be 75%; and 25% if considering only organic sources. At 50 hPa, contributions of iodine from organic and inorganic sources to total iodine-induced ozone loss are found to be compatible. We also verified that even if the

465   concentration of iodine is much less than other halogens it could play a noticeable role in the lower stratospheric ozone depletion especially over high latitudes. Nevertheless, negative lower stratospheric changes recently found by Ball et al. (2018) might be driven by iodine chemistry only in the lowermost stratosphere as the iodine effect in the extratropical lower stratosphere is not supposed to produce such a broad signal. At the same time, SOCOL-AERv2-I suggests that cross-cycles of iodine with bromine and chlorine might sufficiently affect ozone covering the 50-70% of total iodine contribution to ozone reduction in the

470   lower stratosphere at mid-to-high latitudes with a strongest contribution in the Northern hemisphere. It should be noted that the I-Br/I-Cl ratio in the total effect of iodine on ozone requires additional studying. The upper stratospheric ozone is not affected by iodine chemistry similar to the impact of bromine chemistry as presumably, the iodine species in the upper stratosphere are hardly being in active form (IO) than that of chlorine will be in form of ClO due to longer lifetime of chlorine precursors (Daniel et al., 1999). Our results also demonstrate a lowering of the IO mixing ratio in the upper stratosphere. Hence, the net

475 effect is that iodine is relatively more important in the lower stratosphere despite the abundance of total inorganic gas-phase iodine is expected to be similar throughout the stratosphere (see Figure 3).

Also, we would like to address here some shortcomings of the current iodine scheme and further updates that are antici-pated to increase the accuracy of iodine simulations in chemistry-climate models. A strong local decrease in free tropospheric
480 ozone can be expected from iodine collected inside iodized aerosol particles from deserts and oceans which can reach the above-cloud troposphere where they release iodine (Volkamer et al., 2021). However, such complex aerosol iodine chemistry cannot be properly simulated with current chemistry-climate models (Baker, 2004; Sherwen et al., 2016b). The recent studies of Gómez-Martín et al. (2020), Baccarini et al. (2020), and He et al. (2021) suggested that iodine species can make new aerosol particles that are big enough to be cloud condensation nuclei (CCNs). Polar ice-melting in turn leads to the increase of the
485 atmospheric amount of iodine (Cuevas et al., 2018) which may enhance the formation of CCNs. These findings are worth studying further using global climate models with advanced aerosol chemistry and cloud microphysics. Additionally, higher iodine oxides species presented in our study by I_2O_2, I_2O_3, and I_2O_4 might decompose to form iodine oxoacids that growth further to become CCNs (McFiggans et al., 2004; Burkholder et al., 2004; Saunders et al., 2010). However, the formation of iodine oxoacids is still an open question that needs further studying (He et al., 2021). Here, we did not consider any iodine in
490 aerosol form, and these species are represented only in the gas-phase. Also, as was mentioned above, in this work we used a simplified approach for photolysis of higher-order iodine oxides. However, the cross-sections for photolysis of these species are recently measured and can be used to increase the accuracy of simulation (Lewis et al., 2020). Recent field evidence indi-cates that the recycling of iodine on sea-salt aerosol, and perhaps other types of aerosols, may be much faster than currently represented (Tham et al., 2021). Also, we did not include CF_3I that also could modify the total concentration of iodine in the
495 atmosphere. However, based on the recent studies, it will not substantially impact the stratospheric ozone loss showing even less impact than that of CH_3I (Zhang et al., 2020) and will mostly affect the tropical and northern mid-latitudes tropospheric ozone because of higher concentration of pollutants (Youn et al., 2010). All organic iodine emissions in our scheme are pre-scribed. However, they can be interactively calculated in the model utilizing ocean biogenic sources (Ordóñez et al., 2012). It can be embodied also in the next-generation Earth system model where the ocean biosphere is interactively calculated. As it
500 was mentioned above, the sea-surface iodide that is the precursor for HOI/I_2 fluxes has some uncertainty in the models and observations (Chance et al., 2014; Sherwen et al., 2019). However, Shaw and Carpenter (2013) argued that the iodide field does not necessarily solve any uncertainty in the HOI/I_2 flux calculation or other impacts on these fluxes. Nonetheless, there is a prediction for increased iodide that will potentially impact the iodine abundance in the future (Carpenter et al., 2021). Also, there are region-specific parameterizations for sea surface iodide concentration that can be implemented in the next version of
505 the iodine scheme in SOCOL-AERv2-I to increase the reliability of abiotic iodine emissions (Inamdar et al., 2020). Recent investigations of the chemical basis of the HOI/I_2 source can help improve the generalization of empirical source functions (Moreno et al., 2020).

Our sensitivity study showed that the contribution of increased iodine to ozone is almost linear compared to the present-day iodine. To simulate the reliable future impact of iodine on ozone, the recent estimations on future iodine emissions based on

RCP scenarios can be used (Iglesias-Suarez et al., 2020). Tropospheric ozone content in SOCOL-AERv2-I is overestimated compared to other models (Revell et al., 2018) that affects the sea-surface deposition of O_3 and its concentration inside the marine boundary layer, hence the accuracy of simulated iodine emissions. It is planned to fix this problem in future versions of SOCOL.

One of the most controversial parts of atmospheric iodine studies is the scrutiny of the role of volcanic iodine in stratospheric chemistry and its effect on ozone. The volcanic iodine impact is worth studying since some of the powerful volcanoes are supposedly capable to directly inject the iodine into the stratosphere and suppose to result in negative and long-lasting implications for the ozone layer (Bureau et al., 2000; Aiuppa et al., 2005; Balcone-Boissard et al., 2010; Cadoux et al., 2015). However, there is no solid evidence that volcanoes can inject a sufficient amount of iodine into the atmosphere (Schönhardt et al., 2017) and it is needed to organize the measurement campaigns to make estimations of emitted volcanic iodine in a more precise way.

The results of this work showed the highest impact of iodine on ozone in the lowermost stratosphere at high latitudes. This finding indicates the necessity of having broad measurements of iodine species in this region.

We also stress that the iodine can presumably be more noteworthy in the future. The intensified Brewer-Dobson circulation might bring more iodine into the stratosphere in the future than today. Also, the further increase of sea surface temperature due to global warming, near-surface ozone, and sea surface iodide concentrations could be the reason for the intensification of iodine emissions in the future making the atmospheric amount of iodine to be vastly higher (Cuevas et al., 2018; Legrand et al., 2018; Cuevas et al., 2018; Koenig et al., 2020; Iglesias-Suarez et al., 2020; Carpenter et al., 2021). The effectiveness of iodine for ozone destruction is found to be stable in future warming scenarios and therefore its relative importance increases relative to the other halogens (Klobas et al., 2021).

All of this inspires further efforts to better characterize the iodine in the atmosphere and its impact on ozone loss. Alongside, the further improvements of iodine chemistry simulations in chemistry-climate models, it is needed to overcome the scarcity of global measurements of iodine chemistry especially in the upper troposphere and lower stratosphere to increase the accuracy of estimations for iodine impact on ozone loss and to make better predictions of the future ozone evolution.

545   *Competing interests.* The authors declare that they have no conflict of interest.

References

Aiuppa, A., Federico, C., Franco, A., Giudice, G., Gurrieri, S., Inguaggiato, S., Liuzzo, M., McGonigle, A. J. S., and Valenza, M.: Emission of bromine and iodine from Mount Etna volcano, Geochemistry, Geophysics, Geosystems, 6, Q08008, https://doi.org/10.1029/2005GC000965, 2005.

Akagi, S. K., Yokelson, R. J., Wiedinmyer, C., Alvarado, M. J., Reid, J. S., Karl, T., Crounse, J. D., and Wennberg, P. O.: Emission factors for open and domestic biomass burning for use in atmospheric models, Atmospheric Chemistry & Physics, 11, 4039–4072, https://doi.org/10.5194/acp-11-4039-2011, 2011.

Alejandro Barrera, J., Fernandez, R. P., Iglesias-Suarez, F., Cuevas, C. A., Lamarque, J.-F., and Saiz-Lopez, A.: Seasonal impact of biogenic very short-lived bromocarbons on lowermost stratospheric ozone between 60° N and 60° S during the 21st century, Atmospheric Chemistry & Physics, 20, 8083–8102, https://doi.org/10.5194/acp-20-8083-2020, 2020.

Archibald, A., Turnock, S., Griffiths, P., Cox, T., Derwent, R. G., Knote, C., and Shin, M.: On the changes in surface ozone over the twenty-first century: sensitivity to changes in surface temperature and chemical mechanisms., Philosophical transactions. Series A, Mathematical, physical, and engineering sciences, 378, 20190 329, https://doi.org/10.1098/rsta.2019.0329, 2020.

Aschmann, J. and Sinnhuber, B. M.: Contribution of very short-lived substances to stratospheric bromine loading: uncertainties and constraints, Atmospheric Chemistry & Physics, 13, 1203–1219, https://doi.org/10.5194/acp-13-1203-2013, 2013.

Baccarini, A., Karlsson, L., Dommen, J., Duplessis, P., Vüllers, J., Brooks, I. M., Saiz-Lopez, A., Salter, M., Tjernström, M., Baltensperger, U., Zieger, P., and Schmale, J.: Frequent new particle formation over the high Arctic pack ice by enhanced iodine emissions, Nature Communications, 11, 4924, https://doi.org/10.1038/s41467-020-18551-0, 2020.

Badia, A., Reeves, C. E., Baker, A. R., Saiz-Lopez, A., Volkamer, R., Koenig, T. K., Apel, E. C., Hornbrook, R. S., Carpenter, L. J., Andrews, S. J., Sherwen, T., and von Glasow, R.: Importance of reactive halogens in the tropical marine atmosphere: a regional modelling study using WRF-Chem, Atmospheric Chemistry & Physics, 19, 3161–3189, https://doi.org/10.5194/acp-19-3161-2019, 2019.

Baidar, S., Oetjen, H., Coburn, S., Dix, B., Ortega, I., Sinreich, R., and Volkamer, R.: The CU Airborne MAX-DOAS instrument: vertical profiling of aerosol extinction and trace gases, Atmospheric Measurement Techniques, 6, 719–739, https://doi.org/10.5194/amt-6-719-2013, 2013.

Baker, A. R.: Inorganic iodine speciation in tropical Atlantic aerosol, , 31, L23S02, https://doi.org/10.1029/2004GL020144, 2004.

Balcone-Boissard, H., Villemant, B., and Boudon, G.: Behavior of halogens during the degassing of felsic magmas, Geochemistry, Geophysics, Geosystems, 11, Q09005, https://doi.org/10.1029/2010GC003028, 2010.

Ball, W. T., Alsing, J., Mortlock, D. J., Staehelin, J., Haigh, J. D., Peter, T., Tummon, F., Stübi, R., Stenke, A., Anderson, J., Bourassa, A., Davis, S. M., Degenstein, D., Frith, S., Froidevaux, L., Roth, C., Sofieva, V., Wang, R., Wild, J., Yu, P., Ziemke, J. R., and Rozanov, E. V.: Evidence for a continuous decline in lower stratospheric ozone offsetting ozone layer recovery, Atmospheric Chemistry & Physics, 18, 1379–1394, https://doi.org/10.5194/acp-18-1379-2018, 2018.

Bell, N., Hsu, L., Jacob, D. J., Schultz, M. G., Blake, D. R., Butler, J. H., King, D. B., Lobert, J. M., and Maier-Reimer, E.: Methyl iodide: Atmospheric budget and use as a tracer of marine convection in global models, Journal of Geophysical Research (Atmospheres), 107, 4340, https://doi.org/10.1029/2001JD001151, 2002.

Bloss, W. J., Camredon, M., Lee, J. D., Heard, D. E., Plane, J. M. C., Saiz-Lopez, A., Bauguitte, S. J. B., Salmon, R. A., and Jones, A. E.: Coupling of HO_x, NO_x and halogen chemistry in the antarctic boundary layer, Atmospheric Chemistry & Physics, 10, 10 187–10 209, https://doi.org/10.5194/acp-10-10187-2010, 2010.

Bureau, H., Keppler, H., and Métrich, N.: Volcanic degassing of bromine and iodine: experimental fluid/melt partitioning data and applications to stratospheric chemistry, Earth and Planetary Science Letters, 183, 51–60, https://doi.org/10.1016/S0012-821X(00)00258-2, 2000.

Burkholder, J. B., Curtius, J., Ravishankara, A. R., and Lovejoy, E. R.: Laboratory studies of the homogeneous nucleation of iodine oxides, Atmospheric Chemistry & Physics, 4, 19–34, https://doi.org/10.5194/acp-4-19-2004, 2004.

Burkholder, J. B., Sander, S. P., Abbatt, J., Barker, J. R., Huie, R. E., Kolb, C. E., Kurylo, M. J., Orkin, V. L., Wilmouth, D. M., and Wine, P. H.: Chemical Kinetics and Photochemical Data for Use in Atmospheric Studies, JPL, https://doi.org/http://jpldataeval.jpl.nasa.gov, 2015.

Cadoux, A., Scaillet, B., Bekki, S., Oppenheimer, C., and Druitt, T. H.: Stratospheric Ozone destruction by the Bronze-Age Minoan eruption (Santorini Volcano, Greece), Scientific Reports, 5, 12243, https://doi.org/10.1038/srep12243, 2015.

Carpenter, L. J., MacDonald, S. M., Shaw, M. D., Kumar, R., Saunders, R. W., Parthipan, R., Wilson, J., and Plane, J. M. C.: Atmospheric iodine levels influenced by sea surface emissions of inorganic iodine, Nature Geoscience, 6, 108–111, https://doi.org/10.1038/ngeo1687, 2013.

Carpenter, L. J., Chance, R. J., Sherwen, T., Adams, T. J., Ball, S. M., Evans, M. J., Hepach, H., J., H. L. D., Hughes, C., Jickells, T. D., Mahajan, A., Stevens, D. P., Tinel, L., and Wadley, M. R.: Marine iodine emissions in a changing world., Proc. R. Soc. Lond. A., accepted., https://doi.org/http://doi.org/10.1098/rspa.2017.1234, 2021.

Chameides, W. L. and Davis, D. D.: Iodine: Its possible role in tropospheric photochemistry, jgr, 85, 7383–7398, https://doi.org/10.1029/JC085iC12p07383, 1980.

Chance, R., Baker, A. R., Carpenter, L., and Jickells, T. D.: The distribution of iodide at the sea surface, Environ. Sci.: Processes Impacts, 16, 1841–1859, https://doi.org/10.1039/C4EM00139G, 2014.

Chipperfield, M. P., Dhomse, S., Hossaini, R., Feng, W., Santee, M. L., Weber, M., Burrows, J. P., Wild, J. D., Loyola, D., and Coldewey-Egbers, M.: On the Cause of Recent Variations in Lower Stratospheric Ozone, , 45, 5718–5726, https://doi.org/10.1029/2018GL078071, 2018.

Cuevas, C., Maffezzoli, N., and Corella, J. e. a.: Rapid increase in atmospheric iodine levels in the North Atlantic since the mid-20th century., Nat Commun, 9, 1452, https://doi.org/10.1038/s41467-018-03756-1, 2018.

Daniel, J. S., Solomon, S., Portmann, R. W., and Garcia, R. R.: Stratospheric ozone destruction: The importance of bromine relative to chlorine, , 104, 23,871–23,880, https://doi.org/10.1029/1999JD900381, 1999.

Davis, D., Crawford, J., Liu, S., McKeen, S., Band y, A., Thornton, D., Rowland, F., and Blake, D.: Potential impact of iodine on tropospheric levels of ozone and other critical oxidants, jgr, 101, 2135–2147, https://doi.org/10.1029/95JD02727, 1996.

Dix, B., Baidar, S., Bresch, J. F., Hall, S. R., Schmidt, K. S., Wang, S., and Volkamer, R.: Detection of iodine monoxide in the tropical free troposphere, Proceedings of the National Academy of Science, 110, 2035–2040, https://doi.org/10.1073/pnas.1212386110, 2013.

Egorova, T., Rozanov, E., Zubov, V., and Karol, I.: Model for investigating ozone trends (MEZON), Izvestiya - Atmospheric and Ocean Physics, 39, 277–292, 2003.

Egorova, T., Rozanov, E., Gröbner, J., Hauser, M., and Schmutz, W.: Montreal Protocol Benefits simulated with CCM SOCOL, Atmospheric Chemistry & Physics, 13, 3811–3823, https://doi.org/10.5194/acp-13-3811-2013, 2013.

Feinberg, A., Sukhodolov, T., Luo, B.-P., Rozanov, E., Winkel, L. H. E., Peter, T., and Stenke, A.: Improved tropospheric and stratospheric sulfur cycle in the aerosol-chemistry-climate model SOCOL-AERv2, Geoscientific Model Development, 12, 3863–3887, https://doi.org/10.5194/gmd-12-3863-2019, 2019.

Fernandez, R. P., Salawitch, R. J., Kinnison, D. E., Lamarque, J. F., and Saiz-Lopez, A.: Bromine partitioning in the tropical tropopause layer: implications for stratospheric injection, Atmospheric Chemistry & Physics, 14, 13 391–13 410, https://doi.org/10.5194/acp-14-13391-2014, 2014.

Fernandez, R. P., Kinnison, D. E., Lamarque, J.-F., Tilmes, S., and Saiz-Lopez, A.: Impact of biogenic very short-lived bromine on the Antarctic ozone hole during the 21st century, Atmospheric Chemistry & Physics, 17, 1673–1688, https://doi.org/10.5194/acp-17-1673-2017, 2017.

Fuge, R. and Johnson, C. C.: Iodine and human health, the role of environmental geochemistry and diet, a review, Applied Geochemistry, 63, 282–302, https://doi.org/10.1016/j.apgeochem.2015.09.013, 2015.

Gómez-Martín, J. C., Spietz, P., and Burrows, J. P.: Spectroscopic studies of the I2/O3 photochemistry: Part 1: Determination of the absolute absorption cross sections of iodine oxides of atmospheric relevance, Journal of Photochemistry and Photobiology A: Chemistry, 176, 15–38, https://doi.org/https://doi.org/10.1016/j.jphotochem.2005.09.024, https://www.sciencedirect.com/science/article/pii/S1010603005004661, in Honour of Professor Richard P. Wayne, 2005.

Gómez-Martín, J. C., Lewis, T. R., Blitz, M. A., Plane, J. M. C., Kumar, M., Francisco, J. S., and Saiz-Lopez, A.: A gas-to-particle conversion mechanism helps to explain atmospheric particle formation through clustering of iodine oxides, Nature Communications, 11, 4521, https://doi.org/10.1038/s41467-020-18252-8, 2020.

Gravestock, T. J., Blitz, W. J., and Heard, D. E.: A multidimensional study of the reaction CH2I+O2: products and atmospheric implications, Chemphyschem, pp. 3928–3941, https://doi.org/10.1002/cphc.201000575, 2010.

Gutmann, A., Bobrowski, N., Roberts, T. J., Rüdiger, J., and Hoffmann, T.: Advances in bromine speciation in volcanic plumes, Frontiers in Earth Science, 6, 213, https://doi.org/10.3389/feart.2018.00213, 2018.

He, X.-C., Tham, Y. J., Dada, L., Wang, M., Finkenzeller, H., Stolzenburg, D., Iyer, S., Simon, M., Kürten, A., Shen, J., Rörup, B., Rissanen, M., Schobesberger, S., Baalbaki, R., Wang, D. S., Koenig, T. K., Jokinen, T., Sarnela, N., Beck, L. J., Almeida, J., Amanatidis, S., Amorim, A., Ataei, F., Baccarini, A., Bertozzi, B., Bianchi, F., Brilke, S., Caudillo, L., Chen, D., Chiu, R., Chu, B., Dias, A., Ding, A., Dommen, J., Duplissy, J., El Haddad, I., Gonzalez Carracedo, L., Granzin, M., Hansel, A., Heinritzi, M., Hofbauer, V., Junninen, H., Kangasluoma, J., Kemppainen, D., Kim, C., Kong, W., Krechmer, J. E., Kvashin, A., Laitinen, T., Lamkaddam, H., Lee, C. P., Lehtipalo, K., Leiminger, M., Li, Z., Makhmutov, V., Manninen, H. E., Marie, G., Marten, R., Mathot, S., Mauldin, R. L., Mentler, B., Möhler, O., Müller, T., Nie, W., Onnela, A., Petäjä, T., Pfeifer, J., Philippov, M., Ranjithkumar, A., Saiz-Lopez, A., Salma, I., Scholz, W., Schuchmann, S., Schulze, B., Steiner, G., Stozhkov, Y., Tauber, C., Tomé, A., Thakur, R. C., Väisänen, O., Vazquez-Pufleau, M., Wagner, A. C., Wang, Y., Weber, S. K., Winkler, P. M., Wu, Y., Xiao, M., Yan, C., Ye, Q., Ylisirniö, A., Zauner-Wieczorek, M., Zha, Q., Zhou, P., Flagan, R. C., Curtius, J., Baltensperger, U., Kulmala, M., Kerminen, V.-M., Kurtén, T., Donahue, N. M., Volkamer, R., Kirkby, J., Worsnop, D. R., and Sipilä, M.: Role of iodine oxoacids in atmospheric aerosol nucleation, Science, 371, 589–595, https://doi.org/10.1126/science.abe0298, https://science.sciencemag.org/content/371/6529/589, 2021.

Heymsfield, A., Winker, D., Avery, M., Vaughan, M., Diskin, G., Deng, M., Mitev, V., and Matthey, R.: Relationships between Ice Water Content and Volume Extinction Coefficient from In Situ Observations for Temperatures from 0° to -86°C: Implications for Spaceborne Lidar Retrievals*, Journal of Applied Meteorology and Climatology, 53, 479–505, https://doi.org/10.1175/JAMC-D-13-087.1, 2014.

Hilal, S. H., Ayyampalayam, S. N., and Carreira, L. A.: Air-Liquid Partition Coefficient for a Diverse Set of Organic Compounds: Henry's Law Constant in Water and Hexadecane, Environmental Science and Technology, 42, 9231–9236, https://doi.org/10.1021/es8005783, 2008.

Holmes, C. D., Bertram, T. H., Confer, K. L., Graham, K. A., Ronan, A. C., Wirks, C. K., and Shah, V.: The Role of Clouds in the Tropospheric NO$_x$ Cycle: A New Modeling Approach for Cloud Chemistry and Its Global Implications, , 46, 4980–4990, https://doi.org/10.1029/2019GL081990, 2019.

Hossaini, R., Chipperfield, M. P., Montzka, S. A., Rap, A., Dhomse, S., and Feng, W.: Efficiency of short-lived halogens at influencing
670   climate through depletion of stratospheric ozone, Nature Geoscience, 8, 186–190, https://doi.org/10.1038/ngeo2363, 2015.

Iglesias-Suarez, F., Badia, A., Fernandez, R. P., Cuevas, C. A., Kinnison, D. E., Tilmes, S., Lamarque, J.-F., Long, M. C., Hossaini, R., and Saiz-Lopez, A.: Natural halogens buffer tropospheric ozone in a changing climate, Nature Climate Change, 10, 147–154, https://doi.org/10.1038/s41558-019-0675-6, 2020.

Inamdar, S., Tinel, L., Chance, R., Carpenter, L. J., Sabu, P., Chacko, R., Tripathy, S. C., Kerkar, A. U., Sinha, A. K., Venkateswaran
675   Bhaskar, P., Sarkar, A., Roy, R., Sherwen, T., Cuevas, C., Saiz-Lopez, A., Ram, K., and Mahajan, A. S.: Estimation of reactive inorganic iodine fluxes in the Indian and Southern Ocean marine boundary layer, Atmospheric Chemistry & Physics, 20, 12 093–12 114, https://doi.org/10.5194/acp-20-12093-2020, 2020.

Jones, C. E., Hornsby, K. E., Sommariva, R., Dunk, R. M., von Glasow, R., McFiggans, G., and Carpenter, L. J.: Quantifying the contribution of marine organic gases to atmospheric iodine, , 37, L18804, https://doi.org/10.1029/2010GL043990, 2010.

680 Karagodin-Doyennel et al., A.: Aerosol-Chemistry-Climate Model SOCOL-AERv2-iodine code (Version 1.0). Zenodo., https://doi.org/10.5281/zenodo.4844994, 2021a.

Karagodin-Doyennel et al., A.: The iodine chemistry and ozone data simulated with SOCOL AERv2-iodine. Zenodo., https://doi.org/10.5281/zenodo.4820523, 2021b.

Klobas, J. E., Hansen, J., Weisenstein, D. K., Kennedy, R. P., and Wilmouth, D. M.: Sensitivity of Iodine-Mediated Stratospheric Ozone Loss
685   Chemistry to Future Chemistry-Climate Scenarios, frontiers, https://doi.org/10.3389/feart.2021.617586, 2021.

Koenig, T. K., Volkamer, R., Baidar, S., Dix, B., Wang, S., Anderson, D. C., Salawitch, R. J., Wales, P. A., Cuevas, C. A., Fernandez, R. P., Saiz-Lopez, A., Evans, M. J., Sherwen, T., Jacob, D. J., Schmidt, J., Kinnison, D., Lamarque, J.-F., Apel, E. C., Bresch, J. C., Campos, T., Flocke, F. M., Hall, S. R., Honomichl, S. B., Hornbrook, R., Jensen, J. B., Lueb, R., Montzka, D. D., Pan, L. L., Reeves, J. M., Schauffler, S. M., Ullmann, K., Weinheimer, A. J., Atlas, E. L., Donets, V., Navarro, M. A., Riemer, D., Blake, N. J., Chen, D., Huey, L. G., Tanner,
690   D. J., Hanisco, T. F., and Wolfe, G. M.: BrO and inferred Br$_y$ profiles over the western Pacific: relevance of inorganic bromine sources and a Br$_y$ minimum in the aged tropical tropopause layer, Atmospheric Chemistry & Physics, 17, 15 245–15 270, https://doi.org/10.5194/acp-17-15245-2017, 2017.

Koenig, T. K., Baidar, S., Campuzano-Jost, P., Cuevas, C. A., Dix, B., Fernandez, R. P., Guo, H., Hall, S. R., Kinnison, D., Nault, B. A., Ullmann, K., Jimenez, J. L., Saiz-Lopez, A., and Volkamer, R.: Quantitative detection of iodine in the stratosphere, Proceedings of the
695   National Academy of Sciences, https://doi.org/10.1073/pnas.1916828117, https://www.pnas.org/content/early/2020/01/10/1916828117, 2020.

Lee-Taylor, J. and Redeker, K. R.: Reevaluation of global emissions from rice paddies of methyl iodide and other species, grl, 32, L15801, https://doi.org/10.1029/2005GL022918, 2005.

Legrand, M., McConnell, J. R., Preunkert, S., Arienzo, M., Chellman, N., Gleason, K., Sherwen, T., Evans, M. J., and Carpenter, L. J.:
700   Alpine ice evidence of a three-fold increase in atmospheric iodine deposition since 1950 in Europe due to increasing oceanic emissions, Proceedings of the National Academy of Science, 115, 12 136–12 141, https://doi.org/10.1073/pnas.1809867115, 2018.

Lewis, T. R., Gómez Martín, J. C., Blitz, M. A., Cuevas, C. A., Plane, J. M. C., and Saiz-Lopez, A.: Determination of the absorption cross sections of higher-order iodine oxides at 355 and 532 nm, Atmospheric Chemistry & Physics, 20, 10 865–10 887, https://doi.org/10.5194/acp-20-10865-2020, 2020.

705 Lin, S.-J. and Rood, R. B.: Multidimensional Flux-Form Semi-Lagrangian Transport Schemes, Monthly Weather Review, 124, 2046, https://doi.org/10.1175/1520-0493(1996)124<2046:MFFSLT>2.0.CO;2, 1996.

Lovelock, J. E. and Maggs, R. J.: Halogenated Hydrocarbons in and over the Atlantic, , 241, 194–196, https://doi.org/10.1038/241194a0, 1973.

MacDonald, S. M., Gómez Martín, J. C., Chance, R., Warriner, S., Saiz-Lopez, A., Carpenter, L. J., and Plane, J. M. C.: A laboratory
710 characterisation of inorganic iodine emissions from the sea surface: dependence on oceanic variables and parameterisation for global modelling, Atmospheric Chemistry & Physics, 14, 5841–5852, https://doi.org/10.5194/acp-14-5841-2014, 2014.

Manley, S. L., Wang, N.-Y., Walser, M. L., and Cicerone, R. J.: Methyl halide emissions from greenhouse-grown mangroves, grl, 34, L01806, https://doi.org/10.1029/2006GL027777, 2007.

Manzini, E., Giorgetta, M. A., Esch, M., Kornblueh, L., and Roeckner, E.: The Influence of Sea Surface Temperatures on the Northern Winter
715 Stratosphere: Ensemble Simulations with the MAECHAM5 Model, Journal of Climate, 19, 3863, https://doi.org/10.1175/JCLI3826.1, 2006.

McClain, C. R., Feldman, G. C., and Hooker, S. B.: An overview of the SeaWiFS project and strategies for producing a climate research quality global ocean bio-optical time series, Deep Sea Research Part II: Topical Studies in Oceanography, 51, 5–42, https://doi.org/10.1016/j.dsr2.2003.11.001, 2004.

720 McFiggans, G., Plane, J. M. C., Allan, B. J., Carpenter, L. J., Coe, H., and O'Dowd, C.: A modeling study of iodine chemistry in the marine boundary layer, , 105, 14,371–14,385, https://doi.org/10.1029/1999JD901187, 2000.

McFiggans, G., Coe, H., Burgess, R., Allan, J., Cubison, M., Alfarra, M. R., Saunders, R., Saiz-Lopez, A., Plane, J. M. C., Wevill, D., Carpenter, L., Rickard, A. R., and Monks, P. S.: Direct evidence for coastal iodine particles from Laminaria macroalgae - linkage to emissions of molecular iodine, Atmospheric Chemistry & Physics, 4, 701–713, https://doi.org/10.5194/acp-4-701-2004, 2004.

725 Moreno, C., Baeza-Romero, M.-T., Sanz, M., Gálvez, Ó., López Arza, V., Ianni, J. C., and Espíldora, E.: Iodide conversion to iodate in aqueous and solid aerosols exposed to ozone, Physical Chemistry Chemical Physics (Incorporating Faraday Transactions), 22, 5625–5637, https://doi.org/10.1039/C9CP05601G, 2020.

Newman, P. A., Oman, L. D., Douglass, A. R., Fleming, E. L., Frith, S. M., Hurwitz, M. M., Kawa, S. R., Jackman, C. H., Krotkov, N. A., Nash, E. R., Nielsen, J. E., Pawson, S., Stolarski, R. S., and Velders, G. J. M.: What would have happened to the ozone layer if
730 chlorofluorocarbons (CFCs) had not been regulated?, Atmospheric Chemistry & Physics, 9, 2113–2128, 2009.

Ordóñez, C., Lamarque, J. F., Tilmes, S., Kinnison, D. E., Atlas, E. L., Blake, D. R., Sousa Santos, G., Brasseur, G., and Saiz-Lopez, A.: Bromine and iodine chemistry in a global chemistry-climate model: description and evaluation of very short-lived oceanic sources, Atmospheric Chemistry & Physics, 12, 1423–1447, https://doi.org/10.5194/acp-12-1423-2012, 2012.

Pan, L. L., Atlas, E. L., Salawitch, R. J., Honomichl, S. B., Bresch, J. F., Randel, W. J., Apel, E. C., Hornbrook, R. S., Weinheimer, A. J.,
735 Anderson, D. C., Andrews, S. J., Baidar, S., Beaton, S. P., Campos, T. L., Carpenter, L. J., Chen, D., Dix, B., Donets, V., Hall, S. R., Hanisco, T. F., Homeyer, C. R., Huey, L. G., Jensen, J. B., Kaser, L., Kinnison, D. E., Koenig, T. K., Lamarque, J. F., Liu, C., Luo, J., Luo, Z. J., Montzka, D. D., Nicely, J. M., Pierce, R. B., Riemer, D. D., Robinson, T., Romashkin, P., Saiz-Lopez, A., Schauffler, S., Shieh, O., Stell, M. H., Ullmann, K., Vaughan, G., Volkamer, R., and Wolfe, G.: The Convective Transport of Active Species in the Tropics

(CONTRAST) Experiment, Bulletin of the American Meteorological Society, 98, 106–128, https://doi.org/10.1175/BAMS-D-14-00272.1, 2017.

Prados-Roman, C., Cuevas, C. A., Fernandez, R. P., Kinnison, D. E., Lamarque, J. F., and Saiz-Lopez, A.: A negative feedback between anthropogenic ozone pollution and enhanced ocean emissions of iodine, Atmospheric Chemistry & Physics, 15, 2215–2224, https://doi.org/10.5194/acp-15-2215-2015, 2015a.

Prados-Roman, C., Cuevas, C. A., Hay, T., Fernandez, R. P., Mahajan, A. S., Royer, S. J., Galí, M., Simó, R., Dachs, J., Großmann, K., Kinnison, D. E., Lamarque, J. F., and Saiz-Lopez, A.: Iodine oxide in the global marine boundary layer, Atmospheric Chemistry & Physics, 15, 583–593, https://doi.org/10.5194/acp-15-583-2015, 2015b.

Pundt, I., Pommereau, J.-P., Phillips, C., and Lateltin, E.: Upper Limit of Iodine Oxide in the Lower Stratosphere, Journal of Atmospheric Chemistry, 30, 173–185, https://doi.org/10.1023/A:1006071612477, 1998.

Rayner, N. A., Parker, D. E., Horton, E. B., Folland , C. K., Alexander, L. V., Rowell, D. P., Kent, E. C., and Kaplan, A.: Global analyses of sea surface temperature, sea ice, and night marine air temperature since the late nineteenth century, Journal of Geophysical Research (Atmospheres), 108, 4407, https://doi.org/10.1029/2002JD002670, 2003.

Read, K. A., Mahajan, A. S., Carpenter, L. J., Evans, M. J., Faria, B. V. E., Heard, D. E., Hopkins, J. R., Lee, J. D., Moller, S. J., Lewis, A. C., Mendes, L., McQuaid, J. B., Oetjen, H., Saiz-Lopez, A., Pilling, M. J., and Plane, J. M. C.: Extensive halogen-mediated ozone destruction over the tropical Atlantic Ocean, , 453, 1232–1235, https://doi.org/10.1038/nature07035, 2008.

Revell, L. E., Tummon, F., Stenke, A., Sukhodolov, T., Coulon, A., Rozanov, E., Garny, H., Grewe, V., and Peter, T.: Drivers of the tropospheric ozone budget throughout the 21st century under the medium-high climate scenario RCP 6.0, Atmospheric Chemistry & Physics, 15, 5887–5902, https://doi.org/10.5194/acp-15-5887-2015, 2015.

Revell, L. E., Stenke, A., Tummon, F., Feinberg, A., Rozanov, E., Peter, T., Abraham, N. L., Akiyoshi, H., Archibald, A. e. T., Butchart, N., Deushi, M., Jöckel, P., Kinnison, D., Michou, M., Morgenstern, O., O'Connor, F. M., Oman, L. D., Pitari, G., Plummer, D. A., Schofield, R., Stone, K., Tilmes, S., Visioni, D., Yamashita, Y., and Zeng, G.: Tropospheric ozone in CCMI models and Gaussian process emulation to understand biases in the SOCOLv3 chemistry-climate model, Atmospheric Chemistry & Physics, 18, 16 155–16 172, https://doi.org/10.5194/acp-18-16155-2018, 2018.

Saiz-Lopez, A. and Plane, J. M. C.: Novel iodine chemistry in the marine boundary layer, , 31, L04 112, https://doi.org/10.1029/2003GL019215, 2004.

Saiz-Lopez, A., Plane, J. M. C., Baker, A. R., Carpenter, L. J., Von Glasow, R., Gómez Martín, J. C., McFiggans, G., and Saunders, R. W.: Atmospheric Chemistry of Iodine, Chem. Rev., 112, 1773–1804, https://doi.org/10.1021/cr200029u, 2012.

Saiz-Lopez, A., Fernandez, R. P., Ordóñez, C., Kinnison, D. E., Gómez Martín, J. C., Lamarque, J. F., and Tilmes, S.: Iodine chemistry in the troposphere and its effect on ozone, Atmospheric Chemistry & Physics, 14, 13 119–13 143, https://doi.org/10.5194/acp-14-13119-2014, 2014.

Saiz-Lopez, A., Baidar, S., Cuevas, C. A., Koenig, T. K., Fernandez, R. P., Dix, B., Kinnison, D. E., Lamarque, J. F., Rodriguez-Lloveras, X., Campos, T. L., and Volkamer, R.: Injection of iodine to the stratosphere, grl, 42, 6852–6859, https://doi.org/10.1002/2015GL064796, 2015.

Saunders, R. W., Kumar, R., Martín, J. C. G., Mahajan, A. S., Murray, B. J., and Plane, J. M. C.: Studies of the Formation and Growth of Aerosol from Molecular Iodine Precursor, Zeitschrift für Physikalische Chemie, 224, 1095–1117, https://doi.org/doi:10.1524/zpch.2010.6143, https://doi.org/10.1524/zpch.2010.6143, 2010.

Schmidt, J. A., Jacob, D. J., Horowitz, H. M., Hu, L., Sherwen, T., Evans, M. J., Liang, Q., Suleiman, R. M., Oram, D. E., Le Breton, M., Percival, C. J., Wang, S., Dix, B., and Volkamer, R.: Modeling the observed tropospheric BrO background: Importance of multiphase chemistry and implications for ozone, OH, and mercury, Journal of Geophysical Research (Atmospheres), 121, 11,819–11,835, https://doi.org/10.1002/2015JD024229, 2016.

780 Schönhardt, A., Richter, A., Wittrock, F., Kirk, H., Oetjen, H., Roscoe, H. K., and Burrows, J. P.: Observations of iodine monoxide columns from satellite, Atmospheric Chemistry & Physics, 8, 637–653, https://doi.org/10.5194/acp-8-637-2008, 2008.

Schönhardt, A., Richter, A., Theys, N., and Burrows, J. P.: Space-based observation of volcanic iodine monoxide, Atmospheric Chemistry & Physics, 17, 4857–4870, https://doi.org/10.5194/acp-17-4857-2017, 2017.

Shaw, M. D. and Carpenter, L. J.: Modification of Ozone Deposition and I2Emissions at the Air-Aqueous Interface by Dissolved Organic

785 Carbon of Marine Origin, Environmental Science and Technology, 47, 10 947–10 954, https://doi.org/10.1021/es4011459, 2013.

Sheng, J.-X., Weisenstein, D. K., Luo, B.-P., Rozanov, E., Stenke, A., Anet, J., Bingemer, H., and Peter, T.: Global atmospheric sulfur budget under volcanically quiescent conditions: Aerosol-chemistry-climate model predictions and validation, Journal of Geophysical Research (Atmospheres), 120, 256–276, https://doi.org/10.1002/2014JD021985, 2015.

Sherwen, T. M., Evans, M. J., Carpenter, L. J., Andrews, S. J., Lidster, R. T., Dix, B., Koenig, T. K., Sinreich, R., Ortega, I., Volkamer, R.,

790 Saiz-Lopez, A., Prados-Roman, C., Mahajan, A. S., and Ordonez, C.: Iodine's impact on tropospheric oxidants: a global model study in GEOS-Chem, Atmos. Chem. Phys., 16, 1161–1186, https://doi.org/10.5194/acp-16-1161-2016, 2016a.

Sherwen, T. M., Evans, M. J., Spracklen, D. V., Carpenter, L. J., Chance, R., Baker, A. R., Schmidt, J. A., and Breider, T. J.: Global modeling of tropospheric iodine aerosol, , 43, 10,012–10,019, https://doi.org/10.1002/2016GL070062, 2016b.

Sherwen, T. M., Schmidt, J. A., Evans, M. J., Carpenter, L. J., Großmann, K., Eastham, S. D., Jacob, D. J., Dix, B., Koenig, T. K.,

795 Sinreich, R., Ortega, I., Volkamer, R., Saiz-Lopez, A., Prados-Roman, C., Mahajan, A. S., and Ordóñez, C.: Global impacts of tropospheric halogens (Cl, Br, I) on oxidants and composition in GEOS-Chem, Atmospheric Chemistry & Physics, 16, 12 239–12 271, https://doi.org/10.5194/acp-16-12239-2016, 2016c.

Sherwen, T. M., Chance, R. J., Tinel, L., Ellis, D., Evans, M. J., and Carpenter, L. J.: A machine-learning-based global sea-surface iodide distribution, Earth System Science Data, 11, 1239–1262, https://doi.org/10.5194/essd-11-1239-2019, 2019.

800 Sioris, C. E., Kovalenko, L. J., McLinden, C. A., Salawitch, R. J., van Roozendael, M., Goutail, F., Dorf, M., Pfeilsticker, K., Chance, K., von Savigny, C., Liu, X., Kurosu, T. P., Pommereau, J. P., BöSch, H., and Frerick, J.: Latitudinal and vertical distribution of bromine monoxide in the lower stratosphere from Scanning Imaging Absorption Spectrometer for Atmospheric Chartography limb scattering measurements, Journal of Geophysical Research (Atmospheres), 111, D14301, https://doi.org/10.1029/2005JD006479, 2006.

Solomon, S.: Stratospheric ozone depletion: A review of concepts and history, Reviews of Geophysics, 37, 275–316,

805 https://doi.org/10.1029/1999RG900008, 1999.

Solomon, S., Garcia, R. R., and Ravishankara, A. R.: On the role of iodine in ozone depletion, jgr, 99, 20,491–20,499, https://doi.org/10.1029/94JD02028, 1994.

Stenke, A., Schraner, M., Rozanov, E., Egorova, T., Luo, B., and Peter, T.: The SOCOL version 3.0 chemistry-climate model: description, evaluation, and implications from an advanced transport algorithm, Geoscientific Model Development Discussions, 5, 3419–3467,

810 https://doi.org/10.5194/gmdd-5-3419-2012, 2012.

Taylor, K. E., Stouffer, R. J., and Meehl, G. A.: An Overview of CMIP5 and the Experiment Design, Bulletin of the American Meteorological Society, 93, 485–498, https://doi.org/10.1175/BAMS-D-11-00094.1, 2012.

Tham, Y. J., He, X.-C., Li, Q., Cuevas, C. A., Shen, J., Kalliokoski, J., Yan, C., Iyer, S., Lehmusjärvi, T., Jang, S., Thakur, R. C., Beck, L., Kemppainen, D., Olin, M., Sarnela, N., Mikkilä, J., Hakala, J., Marbouti, M., Yao, L., Li, H., Huang, W., Wang, Y., Wimmer, D., Zha, Q., Virkanen, J., Spain, T. G., O'Doherty, S., Jokinen, T., Bianchi, F., Petäjä, T., Worsnop, D. R., Mauldin, R. L., Ovadnevaite, J., Ceburnis, D., Maier, N. M., Kulmala, M., O'Dowd, C., Dal Maso, M., Saiz-Lopez, A., and Sipilä, M.: Direct field evidence of autocatalytic iodine release from atmospheric aerosol, Proceedings of the National Academy of Sciences, 118, https://doi.org/10.1073/pnas.2009951118, https://www.pnas.org/content/118/4/e2009951118, 2021.

Thompson, C. R., Shepson, P. B., Liao, J., Huey, L. G., Apel, E. C., Cantrell, C. A., Flocke, F., Orlando, J., Fried, A., Hall, S. R., Hornbrook, R. S., Knapp, D. J., Mauldin, R. L., I., Montzka, D. D., Sive, B. C., Ullmann, K., Weibring, P., and Weinheimer, A.: Interactions of bromine, chlorine, and iodine photochemistry during ozone depletions in Barrow, Alaska, Atmospheric Chemistry & Physics, 15, 9651–9679, https://doi.org/10.5194/acp-15-9651-2015, 2015.

Vogt, R., Crutzen, P. J., and Sander, R.: A mechanism for halogen release from sea-salt aerosol in the remote marine boundary layer, , 383, 327–330, https://doi.org/10.1038/383327a0, 1996.

Vogt, R., Sander, R., von Glasow, R., and Crutzen, P. J.: Iodine Chemistry and its Role in Halogen Activation and Ozone Loss in the Marine Boundary Layer: A Model Study, Journal of Atmospheric Chemistry, 32, 375–395, https://doi.org/10.1023/A:1006179901037, 1999.

Volkamer, R. and Koenig, K. T.: The CU box-model data (Version 1.0). Zenodo., https://doi.org/10.5281/zenodo.4916787, 2021.

Volkamer, R., Baidar, S., Campos, T. L., Coburn, S., DiGangi, J. P., Dix, B., Eloranta, E. W., Koenig, T. K., Morley, B., Ortega, I., Pierce, B. R., Reeves, M., Sinreich, R., Wang, S., Zondlo, M. A., and Romashkin, P. A.: Aircraft measurements of BrO, IO, glyoxal, NO_2, H_2O, O_2-O_2 and aerosol extinction profiles in the tropics: comparison with aircraft-/ship-based in situ and lidar measurements, Atmospheric Measurement Techniques, 8, 2121–2148, https://doi.org/10.5194/amt-8-2121-2015, 2015.

Volkamer, R., Koenig, T., Apel, E., Bresch, J., Cuevas, C., Dix, B., Eloranta, E., Fernandez, R., Hall, S., Hornbrook, R., Pierce, B., Reeves, M., Saiz-Lopez, A., Spuhler, S., and Ullman, K.: Mini ozone holes due to dust release of iodine, EGU General Assembly 2021, online, https://doi.org/10.5194/egusphere-egu21-13841, 2021.

Wagman, D. D., Evans, W. H., Parker, V. B., Schumm, R. H., Halow, I., Bailey, S. M., Churney, K. L., and Nuttall, R. L.: Erratum: The NBS tables of chemical thermodynamic properties. Selected values for inorganic and C_1 and C_2 organic substances in SI units [J. Phys. Chem. Ref. Data 11, Suppl. 2 (1982)], Journal of Physical and Chemical Reference Data, 18, 1807–1812, https://doi.org/10.1063/1.555845, 1989.

Wang, S., Schmidt, J. A., Baidar, S., Coburn, S., Dix, B., Koenig, T. K., Apel, E., Bowdalo, D., Campos, T. L., Eloranta, E., Evans, M. J., DiGangi, J. P., Zondlo, M. A., Gao, R.-S., Haggerty, J. A., Hall, S. R., Hornbrook, R. S., Jacob, D., Morley, B., Pierce, B., Reeves, M., Romashkin, P., ter Schure, A., and Volkamer, R.: Active and widespread halogen chemistry in the tropical and subtropical free troposphere, Proceedings of the National Academy of Science, 112, 9281–9286, https://doi.org/10.1073/pnas.1505142112, 2015.

Weisenstein, D. K., Yue, G. K., Ko, M. K. W., Sze, N.-D., Rodriguez, J. M., and Scott, C. J.: A two-dimensional model of sulfur species and aerosols, jgr, 102, 13,019–13,035, https://doi.org/10.1029/97JD00901, 1997.

Wittrock, F., Müller, R., Richter, A., Bovensmann, H., and Burrows, J. P.: Measurements of iodine monoxide (IO) above Spitsbergen, Geophys. Res. Lett., 27, 1471–1474, https://doi.org/10.1029/1999GL011146, 2000.

WMO: World Meteorological Organization (WMO). Scientific assessment of ozone depletion: 2014. Geneva, Switzerland, Global Ozone Research and Monitoring Project, 2014.

WMO: World Meteorological Organization (WMO), Executive Summary: Scientific Assessment of Ozone Depletion, Global Ozone Research and Monitoring Project, 86, 2018.

850   Youn, D., Patten, K. O., Wuebbles, D. J., Lee, H., and So, C. W.: Potential impact of iodinated replacement compounds CF_3I and CH_3I on atmospheric ozone: a three-dimensional modeling study, Atmospheric Chemistry & Physics, 10, 10 129–10 144, https://doi.org/10.5194/acp-10-10129-2010, 2010.

Zhang, J., Wuebbles, D. J., Kinnison, D. E., and Saiz-Lopez, A.: Revising the Ozone Depletion Potentials Metric for Short-Lived Chemicals Such as CF_3I and CH_3I, Journal of Geophysical Research (Atmospheres), 125, e32414, https://doi.org/10.1029/2020JD032414, 2020.

855   Zubov, V., Rozanov, E., Egorova, T., Karol, I., and Schmutz, W.: Role of external factors in the evolution of the ozone layer and stratospheric circulation in 21st century, Atmospheric Chemistry & Physics, 13, 4697–4706, https://doi.org/10.5194/acp-13-4697-2013, 2013.